SF3B1 promotes tumor malignancy through splicing-independent co-activation of HIF1α

Patrik T. Simmler[1,6,#], Cédric Cortijo[1,#], Lisa M. Koch[2], Patricia Galliker[1], Silvia Angori[3], Hella A. Bolck[3], Christina Mueller[1], Ana Vukolic[1], Peter Mirtschink[1,+], Yann Christinat[1,°], Natalie R. Davidson[4], Kjong-Van Lehmann[4], Giovanni Pellegrini[5], Chantal Pauli[3], Daniela Lenggenhager[3], Ilaria Guccini[1], Till Ringel[1,6], Christian Hirt[1,6], Gunnar Rätsch[4], Holger Moch[3], Markus Stoffel[1] and Gerald Schwank[1,6*]

[1]Institute of Molecular Health Sciences, ETH Zurich, 8093 Zurich, Switzerland. [2]Institute of Biochemistry, ETH Zurich, 8093 Zurich, Switzerland. [3]Department of Pathology and Molecular Pathology, University Hospital Zurich, 8091 Zurich, Switzerland. [4]Department of Computer Science, ETH Zurich, 8093 Zurich, Switzerland. [5]Institute of Veterinarian Science, University of Zurich, 8057 Zurich, Switzerland. [6]Institute of Pharmacology and Toxicology, University of Zurich, 8057 Zurich, Switzerland.

[#]These authors contributed equally to this work.

*Correspondence: Gerald Schwank (schwank@pharma.uzh.ch)

[+]Present address: Institute of Clinical Chemistry and Laboratory Medicine, Department of Clinical Pathobiochemistry, University Hospital Dresden, 01307 Dresden, Germany. °Present address: Hôpitaux Universitaires de Genève, Service de Pathologie Clinique, Rue Michel-Servet 1, 1206 Genève, Switzerland.

ABSTRACT

Heterozygous mutations in the splicing factor SF3B1 are frequently occurring in various cancers and drive tumor progression through the activation of cryptic splice sites in multiple genes. Recent studies moreover demonstrate a positive correlation between expression levels of wildtype SF3B1 and tumor malignancy, although the underlying mechanisms for this phenomenon remain elusive. Here, we report that SF3B1 acts as a coactivator for hypoxia-inducible factor (HIF)1α through a splicing-independent mechanism. By directly interacting with HIF1α, SF3B1 augments HIF1α-HIF1β heterodimer binding to hypoxia response elements, and facilitates full transcriptional response of HIF target genes. We further validate the relevance of this mechanism for tumor progression, and show that monoallelic deletion of *Sf3b1* impedes pancreatic cancer formation via HIF signaling. Altogether our work demonstrates a pivotal role of SF3B1 in the adaptation to hypoxia, suggesting a causal link between high SF3B1 levels and cancer aggressiveness.

Keywords: hypoxia, HIF transcription, splicing, SF3B1, pancreatic cancer, chromophobe renal cell carcinoma

MAIN

SF3B1 is a core component of the U2 small nuclear ribonucleoprotein (snRNP) complex, involved in the recognition and selection of the branchpoint sequence in RNA splicing[1]. Missense mutations in this gene are frequently found in a number of different blood cancers (e. g. myelodysplastic syndrome, chronic lymphocytic leukemia) and solid tumors (e. g. breast and pancreatic cancers, uveal melanoma)[2,3]. They lead to aberrant 3' splice site usage, resulting in the creation of novel isoforms and/or nonsense mediated decay of hundreds of genes[4–7]. For several of these splice isoforms, a direct tumor promoting function has been demonstrated (i.e. MAP3K7, PPP2R5A)[8–10], confirming the proto-oncogenic role of SF3B1. Interestingly, recent tumor biomarker studies have also found a link between wildtype SF3B1 expression levels and tumor aggressiveness in endometrial-, prostate-, liver- and breast cancer, with higher expression being associated with adverse prognosis[11–14]. Considering that in heart tissue SF3B1 overexpression is induced by hypoxia[15], and that solid cancers are often poorly oxygenated[16], we hypothesized that upregulation of wildtype SF3B1 in tumors facilitates adaptation to hypoxia. In this study we demonstrate that SF3B1 physically interacts with hypoxia inducible factor (HIF)1α to enable full transcriptional response to hypoxia, and show the importance of this mechanism for the progression of hypoxic cancers such as pancreatic ductal adenocarcinoma (PDAC).

We previously observed that SF3B1 is regulated by HIF in ischemic heart conditions[15]. To assess if *SF3B1* is also a HIF target gene in cancer, we first analyzed RNA sequencing (RNA-seq) data in four different solid cancers (PDAC, prostate cancer (PCA), hepatocellular carcinoma (HCC) and breast cancer (BRCA)). Supporting our assumption, we found a close correlation between the expression of *SF3B1* and the two key components of HIF signaling, *HIF1A* and *HIF1B* in all four cancer types (Fig. 1A, B). Similar to the well-described HIF target gene *CA9*[17], we moreover observed a tendency for shorter survival in patients with higher *SF3B1* expression (Fig. 1C). Due to the well-known hypoxic environment found in PDAC[18], we focused on this cancer to further investigate the role of SF3B1 in HIF signaling. In line with the hypothesis that *SF3B1* is a HIF target, we found a strong correlation between the mean expression of 34 known HIF target genes and the expression of *SF3B*1 ($p<0.001$; Fig. 1D). Using a panel of patient-derived PDAC organoids, we furthermore discovered that *SF3B1* expression is significantly upregulated upon experimental induction of hypoxia (Fig. 1E). In addition, expression of a constitutively active variant of HIF1α (HIF1α(ΔΔP)) in a PDAC cell line activated a wildtype *SF3B1*-promoter-luciferase reporter, but not a mutant variant where the hypoxia-response element (HRE) of *SF3B1*-promoter was modified (Fig. 1F).

To next determine whether *SF3B1* is not only a target of HIF signaling but also a regulator of HIF pathway activity, we manipulated *SF3B1* expression levels in multiple human PDAC cell lines and patient-derived PDAC organoids via overexpression, siRNA-mediated knock-down, and monoallelic knockout (Suppl. Fig. 1A, B). While *SF3B1* overexpression caused an increase of VEGF-luciferase reporter activity in a concentration-dependent manner (Fig. 1G, H), and an upregulation of known HIF target genes (Fig. 1I), reduction of *SF3B1* levels led to a significant downregulation of these target genes (Fig. 1I). Notably the strongest downregulation was observed for the prognostic biomarker *CA9*. Together, these data demonstrate that SF3B1 is a modulator of HIF signaling that is transcriptionally regulated by HIF activity.

A study in breast cancer cell lines previously identified a panel of genes prone to intron retention upon *SF3B1* knock-down[19]. Interestingly, heterozygous loss of *SF3B1* in PANC-1 cells did not lead to defective splicing in these genes (Suppl. Fig. 1C), indicating that SF3B1 modulates HIF signaling directly and not indirectly via the activation of cryptic splice sites in HIF pathway components. To test this hypothesis, we assessed whether SF3B1 physically interacts with the core components of HIF signaling HIF1α and HIF1β. Immunoprecipitation assays indeed demonstrated that under hypoxic conditions SF3B1 binds to the HIF1α/HIF1β transcriptional complex (Fig. 2A, B). While depletion of SF3B1 by specific siRNAs did not interfere with binding between HIF1β and HIF1α (Fig. 2C, Suppl. Fig. 1D), siRNA-mediated depletion of HIF1α prevented co-immunoprecipitation of SF3B1 with HIF1β (Fig. 2D, Suppl. Fig. 1E). These data suggest that SF3B1 binds the HIF1α-HIF1β heterodimer via HIF1α, but that this binding is not critical for HIF1α-HIF1β heterodimer formation. To validate these findings, we produced recombinant SF3B1, HIF1α and HIF1β *in vitro* in Sf9 insect cells and mixed the purified proteins prior to analyzing their interactions *in vitro*. In this setting, SF3B1 co-immunoprecipitated with HIF1α and vice versa, irrespective whether HIF1β was present or not (Fig. 2E, F), but did not co-immunoprecipitate with HIF1β (Fig. 2F). We also aimed to identify the relevant domain in HIF1α that mediates binding to SF3B1 by producing a series of deletion mutants of HA-tagged HIF1α (Fig. 2G). Coimmunoprecipitation with endogenous SF3B1 revealed that the bHLH-PAS-A-PAS-B domain is necessary and sufficient for SF3B1 complex formation (Fig. 2H).

Direct binding to the transcription factor HIF1α supports our assumption that SF3B1 modulates HIF signaling independent from its role in pre-mRNA splicing. To further investigate this hypothesis, we immunoprecipitated SF3B1 and HIF1α from hypoxic HEK293 cells, and immunoblotted for the presence of various core splicing components. Indeed, only SF3B1, but not HIF1α, immunoprecipitated with the U2snRNP splicing components SF3B4, SF3B2 and SF3B14 (Fig. 2I). As expected for a transcriptional co-factor of HIF1α, chromatin

immunoprecipitations (ChIP) experiments furthermore revealed that SF3B1 is bound to HREs of various HIF target genes under hypoxic conditions (Fig. 3A), and that this binding was abolished upon knockdown of HIF1α (Fig. 3B). Interestingly, when we next depleted SF3B1 by RNA interference, hypoxia-dependent association of HIF1α and HIF1β with HREs was strongly reduced on a number of HIF target gene promoters (Fig. 3C, D; Suppl. Fig. 1F, G). Together, these results suggest that the interaction of SF3B1 to HIF1α facilitates HIF1α-HIF1β heterodimer binding to HRE domains, enabling full transcriptional HIF response. Notably, we also assessed whether frequently occurring oncogenic mutations in SF3B1 could lead to enhanced binding with HIF1α, thereby improving the ability of cancer cells to adapt to hypoxia. However, when HIF1α was co-immunoprecipitated with oncogenic SF3B1^{K700E}, we observed slightly decreased binding compared to wildtype SF3B1, and reduced HIF target gene expression under hypoxia (Fig. 3E-H). Gene expression analysis in patients with solid cancers moreover showed a consistent trend for lower expression of HIF-target genes in tumors containing *SF3B1*^{K700E} (Suppl. Fig. 1H).

To next investigate the importance of SF3B1-mediated HIF regulation for PDAC progression, we engineered a conditional *Sf3b1* knockout mouse model where we reduced SF3B1 levels by heterozygous deletion of *Sf3b1* (Fig. 4A). The allele was crossed into KPC (*LSL-Kras*$^{G12D/+}$*; LSL-Trp53*$^{R172H/+}$*; Ptf1a-Cre*) mice, where pancreas-specific activation of oncogenic *Kras*^{G12D} and dysfunctional *Trp53* drives PDAC development within 9-14 weeks[20]. As expected, homozygous deletion of *Sf3b1* in the pancreas was not viable, and heterozygous deletion in the KPC background (KPCS) led to a significant reduction in *Sf3b1* gene expression and protein levels (Fig. 4B, Suppl. Fig. 2A, B). While no abnormalities with respect to anatomical appearance and weight of the pancreas were observed in *Sf3b1*$^{+/-}$ mice in the non-cancerogenic *Ptf1a-Cre* background (Suppl. Fig. 2C, D), in the KPC background heterozygous deletion of *Sf3b1* led to significant morphological differences (Suppl. Fig. 2E). At 7 weeks of age 60% of KPC mice but only 2% of the KPCS mice developed PanIN lesions (Suppl. Fig. 2F-I), and at 13 weeks of age 100% of KPC mice developed PanIN lesions or PDAC whereas only 60% of KPCS mice had grade 1 or 2 PanIN lesions (Fig. 4C, D; Suppl. Fig. 2G). Furthermore, KPC mice developed larger tumors (Suppl. Fig. 2J, K), and were associated with considerably shorter survival (Fig. 4F).

While we hypothesized that heterozygous *Sf3b1* deletion inhibits PDAC progression via attenuating HIF activity, impaired splicing could provide an alternative explanation. To discriminate between both scenarios, we established 3D organoid cultures from KP- and KPS animals (Fig. 4G, Suppl. Fig. 3A). This enabled us to analyze ductal tumor cells without stromal cell contamination[21], and to control the oxygen concentration of the environment. We first confirmed that lentiviral transduction of a CRE recombinase induced expression of

KRAS^{G12D}, homozygous deletion of *p53*, and heterozygous deletion of *Sf3b1,* leading to a reduction in *Sf3b1* mRNA and protein levels (Fig. 4H; Suppl. Fig 3B-D). We next analyzed global splicing efficiencies in KPC and KPCS organoids under normoxic and hypoxic conditions, but did not find substantial differences in the percentage of 'spliced in' (PSI) events, including exon skips, alternative 3'and 5' sites, and intron retentions (Fig. 4I, J; Suppl. Fig. 3E-L). In contrast, when we assessed the HIF pathway activity, we observed reduced expression of HIF target genes upon heterozygous *Sf3b1* loss under hypoxia, but not under normoxia (Fig. 4K; Suppl. Fig. 3M). These findings were confirmed *in vivo* by immunohistochemistry in mouse tumors, where the expression of HIF1α as well as the HIF target GLUT1 was reduced in KPCS mice compared to KPC mice (Fig. 4L, M; Suppl. Fig. 3N-Q), and in a functional assay for glycolysis, a metabolic process which is activated by hypoxia. Incubation of organoids with radiolabeled [^{14}C]-2-Deoxy-D-glucose showed no major differences in glucose uptake between KPC and KPCS organoids under normoxic conditions (Suppl. Fig. 3R), but a decrease in glucose uptake in KPCS organoids under hypoxia (Fig. 4N). Supporting these results, KPCS organoids grew significantly slower than KPC organoids in hypoxia but not in normoxia (Fig. 4O, P). Together, our results demonstrate that heterozygous deletion of *Sf3b1* in PDAC does not lead to dysfunctional splicing, but impedes adaptation to hypoxia, highlighting the importance of the SF3B1-HIF1α axis in pancreatic cancer pathogenesis.

Gene expression analysis in TCGA datasets, as well as knock-down experiments in melanoma- and breast cancer cell lines, suggest that SF3B1-dependency for HIF target gene regulation is conserved across different solid cancers (Fig. 1A, B; Suppl. Fig. 4A-D). This prompted us to speculate that frequent loss of heterozygosity in *SF3B1* would only be tolerated in tumors with no or mild hypoxia. To test this hypothesis, we focused on the analysis of chromophobe renal cell carcinoma (chRCC), which shows an exceptional high incidence for heterozygous loss of *SF3B1*-encoding chromosome 2, manifesting in low *SF3B1* expression levels compared to the more frequent clear cell renal carcinoma (ccRCC) and other kidney cancers[22–24] (Fig. 5A). To first confirm that *SF3B1* expression facilitates HIF signaling in chRCC, we established primary cell lines from chRCC biopsies, and performed a siRNA-mediated knockdown of *SF3B1*. Reduction in *SF3B1* levels indeed led to impaired transcriptional response to hypoxia (Fig. 5B). After validating the high frequency of chromosome 2 loss in a cohort of chRCC samples (Swiss-cohort: 60% of patients - Suppl. Fig. 5A, B), we performed IHC stainings to assess HIF1α levels as a surrogate for HIF signaling activity. In line with our hypothesis, 90% of patient samples were negative for HIF1α-staining, with the remaining 10% exhibiting low levels (Fig. 5C, D). In contrast, in samples of clear cell renal cell carcinomas (ccRCC), a kidney cancer known for active HIF signaling[22], moderate or high HIF1α staining was observed in 48% of samples (Fig. 5C, D). Consistent with these results, only 23% of

the ChRCC patients show moderate expression of the HIF target GLUT1 compared to 93% of ccRCC patients (Fig. 5C, D), and genes involved in oxidative phosphorylation, but not glycolysis, were upregulated in chRCC (Fig. 5E). These data support our hypothesis that normoxic cancers can tolerate loss of heterozygosity of *SF3B1*. They could also provide an explanation why only 4%-7% of patients of chRCC display tumor metastasis[23], as for this process adaptation to low oxygen tension is pivotal[25]. Indeed, when we stratified chRCC patients with loss of chromosome 2 into samples with low and high *SF3B1* levels (Fig. 5F; Suppl. Fig. 5C), we observed higher incidences of lymph node spreading (7% vs 43%) and poorer prognosis in the group with upregulated *SF3B1* (Fig. 5G, H).

In summary, we report a novel splicing-independent role of SF3B1 in HIF signaling. Through the interaction with HIF1α, SF3B1 stimulates binding of the HIF1α-HIF1β heterodimer to HRE sequences, and activates transcription of HIF target genes. We further describe that SF3B1-dependent co-activation of HIF is relevant for the progression of hypoxic cancers, suggesting a causal link between high *SF3B1* expression and cancer aggressiveness. HIF signaling regulates several hallmarks of cancer, including cell proliferation, survival, angiogenesis, metabolism, and tumor invasion/metastasis, and its inhibition is therefore considered to be a highly promising treatment approach[16,26,27]. Most HIF inhibitors tested in clinical trials, however, showed low specificity and interfered with other biological processes, leading to dose-limiting side-effects[27]. Since binding of SF3B1 to HIF1α is direct, inhibition of this interaction could sensitize tumor cells to low oxygen environments in a highly specific manner. Together with drugs blocking heterodimerization of HIF1α/HIF1β, such compounds might therefore enable long-term treatment without the occurrence of cross-resistance.

ACKNOWLEDGMENTS

Prof. Wilhelm Krek (W.K., Department of Biology, Institute of Molecular Health Sciences, ETH Zurich, Switzerland), passed away in August 2018. He initiated this project and supervised the experiments until his demise. This manuscript is dedicated to his memory.

AUTHOR CONTRIBUTIONS

P.S., C.C., P.M., W.K. and G.S. conceived the study. P.S. and C.C. designed and executed most of the experiments. G.S., W.K. and M.S. supervised the study. P.S. and G.S. wrote the manuscript with input from all authors. L.M.K. performed the experiments related to mutant SF3B1. C.H., C.P and D.L established human cancer organoid cultures. P.G. and C.M. performed isolation and cell biological characterization of murine organoids. A.V. performed ultrasound imaging and was involved in the in-vivo study. T.R. was involved in the establishment of CRISPR-mediated SF3B1 knockout cell lines. I.G. performed in vitro-experiments. P.S., K.V.L. and Y.C. performed the *in-silico* analysis of HIF and SF3B1 expression in human cancers. N.R.D. analyzed RNA-splicing in organoids. G.P. performed mouse tumor tissue IHC and quantified tumor patterns. H.M., S.A. and H.A.B. performed chRCC tissue staining and evaluation and established chRCC cell lines. H.M. was responsible for diagnosis and analysis of renal tumors. We are particularly grateful to D. Hanahan (EPFL, Lausanne, Switzerland) and T. Jacks (Koch Institute, MIT, Cambridge/MA, USA) for providing mouse cancer cell lines and strains. We thank B. Luikart and W. Kaelin for their plasmid constructs obtained via Addgene. Further support was provided by the Tissue Biobank and the in-situ laboratory of the University Hospital Zurich, as well as the Molecular Genetics Laboratory at the University Children's Hospital Zurich. This work was financed by grants from the Swiss National Science Foundation, the Swiss Cancer League, the Walter Fischli Foundation, the University Research Priority Program (URPP) in Translational Cancer Research (University of Zurich) and the Fritz Thyssen Foundation.

COMPETING INTERESTS

The authors declare no competing interests.

REFERENCES

1. Wahl, M. C., Will, C. L. & Lührmann, R. The Spliceosome: Design Principles of a Dynamic RNP Machine. *Cell* **136**, 701–718 (2009).
2. Quesada, V. *et al.* Exome sequencing identifies recurrent mutations of the splicing factor SF3B1 gene in chronic lymphocytic leukemia. *Nat. Genet.* **44**, 47–52 (2012).
3. Yoshida, K. & Ogawa, S. Splicing factor mutations and cancer. *Wiley Interdiscip. Rev. RNA* **5**, 445–459 (2014).
4. Alsafadi, S. *et al.* Cancer-associated SF3B1 mutations affect alternative splicing by promoting alternative branchpoint usage. *Nat. Commun.* **7**, (2016).
5. Kahles, A. *et al.* Comprehensive Analysis of Alternative Splicing Across Tumors from 8,705 Patients. *Cancer Cell* **34**, 211-224 (2018).
6. Darman, R. B. *et al.* Cancer-Associated SF3B1 Hotspot Mutations Induce Cryptic 3' Splice Site Selection through Use of a Different Branch Point. *Cell Rep.* **13**, 1033–1045 (2015).
7. Obeng, E. A. *et al.* Physiologic Expression of Sf3b1K700E Causes Impaired Erythropoiesis, Aberrant Splicing, and Sensitivity to Therapeutic Spliceosome Modulation. *Cancer Cell* **30**, 404–417 (2016).
8. Liu, Z. *et al.* Mutations in the RNA splicing factor SF3B1 promote tumorigenesis through MYC stabilization. *Cancer Discov.* **10**, 806–821 (2020).
9. Liu, B. *et al.* Mutant SF3B1 promotes AKT and NF-kB driven mammary tumorigenesis. *J. Clin. Invest.* (2020).
10. Lieu, Y. K. *et al.* SF3B1 mutant-induced missplicing of MAP3K7 causes anemia in myelodysplastic syndromes. *bioRxiv* (2020).
11. Popli, P. *et al.* Splicing factor SF3B1 promotes endometrial cancer progression via regulating KSR2 RNA maturation. *Cell Death Dis.* **11**, 1–13 (2020).
12. Jiménez-Vacas, J. M. *et al.* Spliceosome component SF3B1 as novel prognostic biomarker and therapeutic target for prostate cancer. *Transl. Res.* **212**, 89–103 (2019).
13. López-Cánovas, J. L. *et al.* Splicing factor SF3B1 is overexpressed and implicated in the aggressiveness and survival of hepatocellular carcinoma. *Cancer Lett.* **496**, 72–83 (2021).
14. Zhang, L. *et al.* Knockdown of SF3B1 inhibits cell proliferation, invasion and migration triggering apoptosis in breast cancer via aberrant splicing. *Breast Cancer* **27**, 464–476 (2020).

15. Mirtschink, P. *et al.* HIF-driven SF3B1 induces KHK-C to enforce fructolysis and heart disease. *Nature* **522**, 444–449 (2015).

16. Semenza, G. L. Targeting HIF-1 for cancer therapy. *Nat. Rev. Cancer* **3**, 721–732 (2003).

17. Yang, L. *et al.* Overexpression of FZD1 and CAIX are Associated with Invasion, Metastasis, and Poor-Prognosis of the Pancreatic Ductal Adenocarcinoma. *Pathol. Oncol. Res.* **24**, 899–906 (2018).

18. Koong, A. C. *et al.* Pancreatic tumors show high levels of hypoxia. *Int. J. Radiat. Oncol. Biol. Phys.* **48**, 919–922 (2000).

19. Paolella, B. R. *et al.* Copy-number and gene dependency analysis reveals partial copy loss of wild-type SF3B1 as a novel cancer vulnerability. *Elife* **6**, 1–28 (2017).

20. Hingorani, S. R. *et al.* Trp53 R172H and Kras G12D cooperate to promote chromosomal instability and widely metastatic pancreatic ductal adenocarcinoma in mice. *Cancer Cell* **7**, 469–483 (2005).

21. Boj, S. F. *et al.* Organoid Models of Human and Mouse Ductal Pancreatic Cancer. *Cell* **160**, 324–338 (2015).

22. Creighton, C. J. *et al.* Comprehensivemolecular characterization of clear cell renal cell carcinoma. *Nature* **499**, 43–49 (2013).

23. Davis, C. F. *et al.* The somatic genomic landscape of chromophobe renal cell carcinoma. *Cancer Cell* **26**, 319–330 (2014).

24. Ohashi, R. *et al.* Allele Loss and Reduced Expression of CYCLOPS Genes is a Characteristic Feature of Chromophobe Renal Cell Carcinoma. *Transl. Oncol.* **12**, 1131–1137 (2019).

25. Ohta, A. *et al.* In vivo T cell activation in lymphoid tissues is inhibited in the oxygen-poor microenvironment. *Front. Immunol.* **2**, (2011).

26. Muz, B., de la Puente, P., Azab, F. & Azab, A. K. The role of hypoxia in cancer progression, angiogenesis, metastasis and resistance to therapy. *Hypoxia* **3**, 83–92 (2015).

27. Semenza, G. L. Pharmacologic targeting of hypoxia-inducible factors. *Annu. Rev. Pharmacol. Toxicol.* **59**, 379–403 (2019).

28. Kahles, A., Ong, C. S., Zhong, Y. & Rätsch, G. SplAdder: Identification, quantification and testing of alternative splicing events from RNA-Seq data. *Bioinformatics* **32**, 1840–1847 (2016).

29. Uhlen, M. *et al.* A pathology atlas of the human cancer transcriptome. *Science* **357**, 660–671 (2017).

30. Cerami, E. *et al.* The cBio Cancer Genomics Portal: An Open Platform for Exploring Multidimensional Cancer Genomics Data. *Cancer Discov.* **32**, 736–740 (2017).

31. Gao, J. *et al.* Integrative Analysis of Complex Cancer Genomics and Clinical Profiles Using the cBioPortal Complementary Data Sources and Analysis Options. *Sci Signal* **6**, 1–20 (2014).

32. Bolck, H. A. *et al.* Cancer Sample Biobanking at the Next Level: Combining Tissue With Living Cell Repositories to Promote Precision Medicine. *Front. Cell Dev. Biol.* **7**, 1–10 (2019).

33. Dahinden, C. *et al.* Mining Tissue Microarray Data to Uncover Combinations of Biomarker Expression Patterns that Improve Intermediate Staging and Grading of Clear Cell Renal Cell Cancer Clinical Cancer Research. *Clin Cancer Res* **16**, 88–98 (2010).

34. Struckmann, K. *et al.* pVHL co-ordinately regulates CXCR4/CXCL12 and MMP2/MMP9 expression in human clear-cell renal cell carcinoma. *J. Pathol.* **214**, 464–471 (2008).

35. Hruban, R. H. *et al.* Pathology of genetically engineered mouse models of pancreatic exocrine cancer: Consensus report and recommendations. *Cancer Res.* **66**, 95–106 (2006).

36. Shalem, O., Sanjana, E. N., Hartenian, E. & Zhang, F. Genome-Scale CRISPR-Cas9 Knockout. *Science* **343**, 84–88 (2014).

37. Huch, M. *et al.* Unlimited in vitro expansion of adult bi-potent pancreas progenitors through the Lgr5/R-spondin axis. *EMBO J.* **32**, 2708–2721 (2013).

METHODS

TCGA data analysis

TCGA RNA-seq expression and clinical data were downloaded either from the TCGA website (https://tcga-data.nci.nih.gov), from The Human Protein Atlas[29] (https://proteinatlas.org) or from The cBio Cancer Genomics Portal[30,31] (https://cbioportal.org). For survival analysis, patients were stratified by the median of *SF3B1* gene expression, except for the chRCC analysis. There, the upper quartile of *SF3B1* expression in patients with chromosome 2 loss was used for stratification. In the survival analysis of chRCC patients, a missing variable (months) of one deceased patient in the *Chr2 loss, SF3B1 high* cohort was imputed by using the mean value of all deceased patients in the unstratified dataset. The hypoxia signature was computed as the average expression of 34 hypoxia-inducible genes represented by *CA9, NDUFA4L2, EGLN3, NDRG1, PFKFB4, ADM, NRN1, CA12, ENO2, ZNF395, RAB20, DDIT4, SLC7A5, BNIP3, HMOX1, POU5F1, ALDOC, PDK1, LDHA, SLC2A1, BNIP3L, STC2, HK2, CP, LOX, MUC1, VEGFA, SLC16A3, MXI1, GYS1, COL5A1, PPP1R3C, TXNIP, LRP1*. K700E mutations are based on a uniform recalled variant dataset. RNA-seq data has been uniformly re-aligned across all 8255 cancer patient samples. Only non-alternate axons are used for gene expression quantification that has been quantile normalised[5]. Data has been made available here: https://gdc.cancer.gov/about-data/publications/PanCanAtlas-Splicing-2018.

Cell culture

SK-MEL-28, PANC-1, MDA-MB-231, Mia-PaCa-2 and HEK293T cells were maintained in Dulbecco's modified Eagle's medium (DMEM, Invitrogen) supplemented with 10% FBS, and 4 mM L-glutamine. AsPC-1 and BxPC-3 cells were maintained in Roswell Park Memorial Institute (RPMI, Invitrogen) supplemented with 10% FBS and 4 mM L-glutamine. Cell lines were cultured at 37 °C in 5% CO_2. Sf9 insect cells were grown in suspension at 27°C in Sf-900 II SFM medium (Invitrogen) supplemented with penicillin/streptomycin (Sigma-Aldrich). Cell density was monitored regularly and was maintained between 0.5 and 2 x10^6 cells/ml. All cell lines have been authenticated by Microsynth and regular mycoplasma tests were performed using the ScienCell Mycoplasma PCR detection kit (Cat. No. 8208).

Quantitative real-time PCR analysis

RNA was isolated using the nucleospin RNA kit (Macherey-Nagel) and reverse-transcribed to cDNA (kit: Applied Biosystems, ref. 43698813). SYBR-green based quantitative real-time PCR (qRT–PCR) was performed on a

LightCycler 480 (Roche). C_t values were normalized to the housekeeping gene *TBP* for human samples and to *Actb* or *Ccny* for the mouse samples. Primer sequences are listed in Supplementary Table 4.

Luciferase assays

Cells were co-transfected with a *Vegf*-HRE-luciferase reporter plasmid, or a *Sf3b1*-HRE-luciferase reporter plasmid together with different plasmids using lipofectamine 2000 (Invitrogen). A renilla luciferase plasmid was co-transfected for internal control. Cells were collected 24 hrs after transfection, and luciferase activity analyzed on a TECAN M1000 PRO using the dual-luciferase reporter assay system (Promega E1980). The assays were carried out according to the manufacturer's instructions.

Transient transfections

siRNAs were transfected using Lipofectamine-RNAiMax reagent (Invitrogen). We used Qiagen human si*SF3B1*#1 (SI04159456), human si*SF3B1*#2 (SI04161766) and human si*HIF1A 5'*-CUG AUG ACC AGC AAC UUG A-3' and 5'-UCA AGU UGC UGG UCA UCA G-3'. For transient overexpression studies, DNA plasmids were transfected with Lipofectamine 2000 (Invitrogen) according to the manufacturer's protocol.

Lentivirus production and transduction

Lentiviral particles were produced in HEK-293T cells. HEK-293T cells were purchased from American Type Culture Collection (ATCC). Cells were transduced with lentivirus by adding virus-containing supernatants to the cell culture medium.

Chromatin immunoprecipitations (ChIP)

ChIP assays were performed with material from HEK293T and the assays carried out using the ChIP-IT Kit (Active Motif) according to the manufacturer's instructions. ChIP was performed with a HIF1α antibody from Abcam (ab2185), a SF3B1 antibody from MBL International (D221-3), an HIF1α antibody from Novus Biological (NB 100-124), or an anti-IgG antibody from Abcam (ab171870). Primer sequences used are listed in Supplementary Table 4.

Immunoblotting and antibodies

Protein lysates were resolved on polyacrylamide minigels and transferred onto nitrocellulose membrane by semi-dry transfer. The following antibodies were used for immunoblotting: rabbit HIF1α (catalogue no. NB-100-479;

Novus Biologicals), mouse SF3B1 (catalogue no. D221-3; MBL International), mouse HIF1α (catalogue no. NB 100-124; Novus Biologicals), mouse SF3B2 (catalogue no. ab56800; Abcam), rabbit SF3B4 (catalogue no. ab157117; Abcam), rabbit SF3B14 (catalogue no. NBP1-87431; Novus Biologicals), rabbit α-tubulin (catalogue no. ab18251; Abcam), rabbit CA9 (catalogue no. NB-100-417; Novus), rabbit PKM2 (catalogue no. 3198; Cell Signaling), rabbit PDK1 (catalogue no. 3061S; Cell Signaling), mouse HA-tag (catalogue no. 26183; Thermo Scientific), rabbit p53 (catalogue no. FL-393; Santa Cruz), mouse KrasG12D (catalogue no. 26036; Neweastbio), mouse total-Ras (catalogue no. 3965; Cell Signaling), rabbit p-Mek (catalogue no. 9154; Cell Signaling), rabbit total-Mek (catalogue no. 9122S; Cell Signaling), rabbit p21 (catalogue no. ab109199; Abcam), rabbit p16 (catalogue no. ab51243; Abcam). Immunodetection and visualization of signals by chemiluminescence was carried out by using the ImageQuant LAS 4000 mini (GE Healthcare). For immunoprecipitation, transfected cells were lysed in cell lysis buffer TNN (50 mM Tris-HCl pH 7.5, 250 mM NaCl, 5 mM EDTA, 0.5% NP-40, 50 mM NaF, 1 mMDTT, 1 mM PMSF, and protease inhibitor cocktail) for 30 min. Magnetic dynabeads (Invitrogen) were incubated first with the primary antibody for 10 min at room temperature, washed and then incubated with the cell lysate for 3 hours at 4°C. The assays were carried out according to the manufacturer's instructions. Finally, the beads were boiled in 2x sample buffer for 5 min and eluents were analyzed by Western blotting. For co-immunoprecipitation with recombinant proteins, magnetic dynabeads (Invitrogen) were incubated first with the primary antibody and then incubated with the recombinant proteins for 2 hours at 4°C.

Human PDAC organoid culture

Human PDAC organoids were established from patients' surgical specimens and cultured as described in full detail by (Hirt *et al*, manuscript under revision). Human pancreatic tissue samples were provided by the Department of Pathology and Molecular Pathology, University Hospital Zurich, based on informed consent and study approval from the ethical committee (BASEC-Nr. 2017-01319). For all samples, the diagnosis of PDAC was confirmed on corresponding tissue slides reviewed by board-certified pathologists. To establish organoid lines, tissue was chopped and digested in full medium containing collagenase type II (5 mg/ml). The digestion was stopped with advanced DMEM/F12 medium supplemented with HEPES (10mM), Glutamax (1%) and penicillin/streptomycin (1%). Cells were seeded as 20µl drops of Matrigel (Corning, growth factor reduced) into a 48-well suspension culture plate. Human PDAC organoids were cultured in Advanced DMEM supplemented with 10×10^{-3} M HEPES, 1x Glutamax, 1% Penicillin/Streptomycin, 1x B27, 1.25×10^{-3} M N-acetylcysteine, 50% Wnt3a conditioned medium (CM), 10% R-spondin-1 CM, 10% noggin CM, 10×10^{-3} M nicotinamide, 1 × 10−6 M prostaglandin E2, 50 ng mL^{-1}, EGF, 10×10^{-9} M gastrin, 100 ng mL^{-1} FGF10 and 0.5×10^{-6} M A83-01.

RCC ethics statement and patient selection

All tissue samples were made available by the Tissue Biobank of the Department of Pathology and Molecular Pathology, University Hospital of Zurich, Switzerland and collected as described previously[32]. The local ethics commission approved this study (BASEC_2019-01959) and patients gave written consent. The retrospective use of normal and tumor tissues of RCC patients is in accordance with the Swiss Human Research Act, which allows the use of biomaterial and patient data for research purposes without informed consent under certain conditions that include the present cases (article 34). All tumors were reviewed by a board-certified pathologist and histologically classified according to the World Health Organization guidelines.

ChRCC tissue processing and generation of cell models

Renal tumors were surgically resected and underwent routine tissue processing and rapid sectioning for diagnostic purposes and generation of cell models (including formalin fixation and paraffin embedding, snap freezing of fresh tumor and normal tissue). Fresh tissue samples macroscopically identified as cancer by a pathologist with specialization in uropathology (H. Moch) were placed into sterile 50-ml conical tubes containing transport media (RPMI (Gibco, Waltham, MA) with 10 % fetal calf serum (FCS, Gibco) and Antibiotic-Antimycotic® (Gibco)) and stored at 4 °C until further processing. Briefly, samples were rinsed with PBS and subsequently cells were isolated by finely cutting the tissue into small pieces followed by collagenase A digestion for 1-3 hours at 37 °C. The slurry was passed through a 100 µm cell strainer to remove large fragments and the Collagenase A digestion was quenched with DMEM containing 10-20 % FCS. Cells were washed once with PBS and if necessary, erythrocytes were lysed. Finally, cell viability was evaluated by trypan blue dye exclusion and an appropriate number of cells was resuspended in Renal Epithelial Cell Growth Medium 2 (Promocell). This suspension was seeded into collagen I-coated cell culture dishes (Corning, Corning, NY) containing 30–50 % confluent Mitomycin C-treated mouse embryonic fibroblasts CF6 (ThermoFisher). Subsequently, the co-culture was maintained in Renal Epithelial Cell Growth Medium 2 in a humidified incubator at 37 °C with 5% CO_2. The medium was replaced earliest 5 days after initial plating and subsequently every three to four days. Cells were expanded by passaging without the addition of new CF6 feeder cells in subsequent passages.

RCC immunohistochemistry

For immunohistochemical (IHC) analyses, a tissue microarray (TMA) and whole tissue sections of primary RCCs from the Department of Pathology and Molecular Pathology, University Hospital of Zurich, Switzerland were

used[33]. Clinicopathological parameters of the RCC specimens are described in Supplementary Table 3. Formalin-fixed paraffin-embedded (FFPE) cell pellets from cell cultures were prepared as previously described[34]. For histological evaluation, FFPE specimens were sectioned (2 µm) and stained with hematoxylin and eosin (HE). For IHC, 2 µm sections were transferred to glass slides followed by antigen retrieval. Antibodies used for IHC are summarized in the table below. IHC was performed using the Ventana Benchmark automated system (Roche, Ventana Medical Systems, Oro Valley, AZ) and Ventana reagents. The Optiview DAB IHC detection and the Discovery Chromomap DAB Kits (Roche, Ventana Medical Systems) were used to stain with the antibodies against Glut1 and SF3B1, respectively. The staining procedure for HIF1α was carried out with the automated Leica BOND system using the Bond Polymer Refine Detection Kit (Leica Biosystems, Wetzlar, Germany).

Antibody	Name/Clone	Dilution IHC	Supplier
SF3B1	EPR11986	1:100	Abcam
HIF1α	HIF-1 alpha antibody [mgc3]	1:400	Abcam
GLUT1	Glucose Transporter type 1	1:1000	Millipore

RNA-extraction of chRCC patient samples

RNA extraction from FFPE specimens of chRCC was performed using the Maxwell® 16 Tissue DNA Purification Kit (Promega). RNA quality was assessed with the RNA Qubit™ RNA HS Assay Kit (ThermoFisher). Subsequently, cDNA was prepared using the Superscript IV Vilo Mastermix (Thermo Fisher).

SF3B1 quantification in chRCC patient samples

The quantitative measurements of SF3B1 were performed using the Taqman Fast Advanced master mix (Thermo Fisher) with 5 ng/µL ng of cDNA in each technical duplicate and the cycling parameters according to the protocol on a ViiA7 (Thermo Fisher). Primer and probe set assay IDs for the TaqMan assays were Hs00961640_g1 for SF3B1 and Hs03929097 for GAPDH, (ThermoFisher). Normal tissue was used to normalize the quantitative analysis of all samples. For the other genes assessed, regular qPCR was performed as described above.

Analysis of Copy Number Variations (CNVs)

DNA was processed and hybridized to Affymetrix CytoScan HD array according to manufacturer's protocol. Sample level quality control was initially assessed by Affymetric ChAS software, version 2.0 and probeset.txt files were exported. These served as input for the *rCGH* R package (v. 3.8) obtained from Bioconductor. The comprehensive comparative genomic hybridization (CGH) analysis workflow provided by *rCGH* was used for log2 relative ratio (LRR) calculation (the sample DNA signals against a normal two-copy DNA reference), profile

centralization and profile segmentation. Significant focal copy number alterations were identified from segmented data using GISTIC 2.05. Subsequently, absolute copy numbers were inferred.

Plasmid design

Deletion mutants of HIF1α were generated by PCR using a pcDNA3-HA-HIF1α plasmid (addgene 18949) as template. We designed specific primers that border the domain to be deleted on both sides in order to remove the different targeted domains of HIF1α.

Baculovirus expression system

Baculovirus expression vectors expressing Strep-Tag II epitope tagged-SF3B1, HIF1α, or HIF1β were constructed by inserting the cDNA of corresponding genes into a pFBDM plasmid. Strep-Tag II tagged-SF3B1, HIF1α, or HIF1β were expressed in Sf9 cells that had been infected with recombinant baculovirus as described in the Bac-to-Bac® Baculovirus Expression System from Invitrogen.

Co-immunoprecipitation assays

Transfected cells were lysed in cell lysis buffer TNN (50mM Tris-HCl pH 7.5, 250 mM NaCl, 5 mM EDTA, 0.5% NP-40, 50 mM NaF, 1 mM DTT, 1 mm PMSF, and protease inhibitor cocktail) for 30 min. Magnetic dynabeads (Invitrogen) were incubated first with the primary antibody for 10 min at room temperature, washed and then incubated with the cell lysate for 3 hours at 4°C. The assays were carried according to the manufacturer's instructions. Finally, the beads were boiled in 2x sample buffer for 5 min. The eluents were analyzed by Western blotting. For co-immunoprecipitations with recombinant proteins, magnetic dynabeads (Invitrogen) were incubated first with the primary antibody, then incubated with the recombinant proteins for 2 hours at 4°C.

Mouse strains

LSL-Kras$^{G12D/+}$*; LSL-Trp53*^{R172H} (KP), and *LSL-Kras*$^{G12D/+}$*; LSL-Trp53*$^{R172H/+}$*; Ptf1a-Cre* (KPC) were obtained from Tyler Jack's (Howard Hughes Medical Institute). Sf3b1 flox/flox mice were generated by targeting exon five and six of the Sf3b1 gene. These exons were floxed with LoxP sites and the targeted region was about 3.0 kb. A LoxP/FRT-flanked neomycin resistance cassette was placed 277 bp upstream of exon five and six for selection. Chimeric mice were generated via electroporation in embryonic stem cells followed by microinjection in blastocysts and implantation into foster mice. For all *in vivo* experiments, except the survival experiment, mice

between the age of 7 and 13 weeks were used. Female and male mice were used for all experiments. All mice were maintained in a SPF animal facility at the ETH Phenomics Center EPIC at ETH Zürich. Maintenance and animal experiments were conducted in accordance with the Swiss Federal Veterinary Office (BVET) guidelines. Animal surgeries and ultrasound (Vevo 2100 system) analysis was performed blinded by a veterinarian. Animal numbers for experiments were chosen based on expected mortality rates and phenotypical changes of the pancreas in mice.

Histological and immunohistochemical analysis (murine specimen)

Following euthanasia, pancreata were removed, weighed and fixed overnight in 10% neutral buffered formalin (Formafix Switzerland AG, Hittnau, Switzerland). The tissue was embedded in paraffin and cut serially into 3-5-µm sections, which were stained with hematoxylin and eosin (HE) and Masson trichrome for the assessment of fibrosis. Histological analysis, including murine pancreatic intraepithelial neoplasia (mPanIN) grading and assessment of the proportion of affected versus unremarkable pancreatic parenchyma, was carried out in the HE-stained sections in a blinded fashion by an ECVP-board certified veterinary pathologist (GP), according to previously reported criteria[35]. Immunohistochemistry (IHC) was conducted on consecutive paraffin-embedded sections using the primary antibodies against HIF1α (rabbit polyclonal, Novus Biological, NB100-479, 1:500), SF3B1 (rabbit monoclonal, clone number EPR11986, Abcam, ab172634, 1:100), GLUT-1 (rabbit polyclonal, Merck Millipore, #400060, 1:100), Ki-67 (rabbit monoclonal, clone name 30-9, Ventana Roche, 790-4286, 1:400), cleaved caspase 3 (rabbit monoclonal, clone number D3E9, Cell Signaling, Cell Signaling, #9579, 1:400) and CD31 (rabbit polyclonal, Santa Cruz, sc-1506R, 1:1000). All immunostains were performed in Ventana Discovery (Ki-67 and cleaved caspase 3) or Dako autostainers using 3,3' diaminobenzidine (DAB) chromogen (Dako-Agilent Technologies, Denmark). All slides were scanned using digital slide scanner NanoZoomer-XR C12000 (Hamamatsu, Japan) and images were taken using NDP.view2 viewing software (Hamamatsu). mPanIN were counted manually in 10 high power fields (HPF) in each HE-stained section. Automated quantitative analysis was carried out on the digital slides using the Visiopharm Integrator System (VIS, version 4.5.1.324, Visiopharm, Hørsholm, Denmark). Briefly, a linear threshold classification allowed recognition of the blue (Masson trichrome) or DAB brown (IHC) structures in 20 regions of interest (ROI) sized 0.237 mm^2 (the area of an HPF with one ocular of 22 mm field of view), randomly selected across the pancreatic parenchyma. Results were expressed as percentage of positive area/ROI vs total parenchyma/ROI (Masson trichrome, HIF-1α, GLUT1, CD31) or average number of positive nuclei or cells/ROI (SF3B1, Ki-67, cleaved caspase 3).

Heterozygous knockout of SF3B1 by CRISPR-Cas9

We used the sgRNA-Designer platform by the Broad Institute to design sgRNAs for targeted gene knock-out (https://portals.broadinstitute.org/gpp/public/analysis-tools/sgRNA-design). Two distinct sgRNAs were used: sgSF3B1_A (5'-TAATCTTCATCAATCAATAG-3') and sgSF3B1_B (5'-AAGATCGCCAAGACTCACGA-3'). According to the protocol from Shalem et al., we adapted the sgRNA design for subsequent cloning into the LentiCRISPRv2 backbone[36]. Cells were transduced with lentivirus and selected with puromycin. Heterozygous knock-out of the target gene was validated with deep sequencing for PANC-1 and AsPC-1 cells at two distinct time-points, to assess the enrichment of in-frame indels. Primers were designed flanking the predicted sgRNA cut-site and containing primer binding sites for Illumina TruSeq Deep sequencing primers. After purification, the amplicons were sequenced on an Illumina MiSeq System, with a minimum of 5'000 reads. Analysis of editing events was performed with CRISPResso V1.0.1.

Murine pancreatic ductal organoid culture

Pancreatic ducts were isolated from the whole organ of 13 weeks old KP and KPS mice as previously described[37]. Each organoid line was isolated from an individual mouse. Isolated ducts as well as the ensuing organoids were embedded in growth-factor reduced (GFR)-Matrigel (Corning), and cultured in organoid medium (OM), which is composed of AdDMEM/F12 (Gibco) supplemented with GlutaMAX (Gibco), HEPES (Gibco), Penicillin-Streptomycin (Invitrogen), B27 (Gibco), N-2 (Gibco), 1.25 mM N-Acetyl-L-cysteine (Sigma), 10 nM Gastrin I (Sigma) and the growth factors: 100 ng/ml FGF10 (Peprotech), 50 ng/ml EGF (Peprotech), 100 ng/ml Noggin, 100 ng/ml RSPO-1 (Peprotech), and 10 mM Nicotinamide (Sigma). For the first week after duct isolation the culture medium was supplemented with 100 µg/ml Primocin (InvivoGen).

Lentiviral production and transduction of organoids

The plasmids FUG-T2A-GFP-Cre and control GFP were purchased from Addgene #66691 and lentiviral particles were produced in HEK-293T cells using X-tremeGene 9 DNA Transfection Reagent (Roche). Upon ultracentrifugation concentrated virus particles were stored at -80°C and used to infect pancreatic ductal organoid cultures as previously described[37]. Briefly, upon dissociation of the GFR-Matrigel, organoid cultures were broken down into single cells using TrypLE Express (Gibco) and fire-polished glass Pasteur pipettes. Single cells were transferred to maximum recovery microtubes (Axygen) and centrifuged at 800 g for 5 min at 4°C. The pellets were resuspended in 250 µl OM and inoculated with 10 µl of concentrated virus particles that was then incubated

at 37°C for 4-6 h. After a washing step, the cells were seeded in GFR-Matrigel and grown in OM. Two to three weeks later the pool of GFP-expressing organoids was dissociated again into single cells and subjected to FACS analysis (MoFlo® Astrios™ EQ) to sort for GFP-positive cells. The cells were put back into culture and used for subsequent experiments.

Organoid proliferation assay

Organoids were seeded as single cells at a density of 500 cells/µl GFR-Matrigel (Corning). 48 hours after seeding, cells were exposed to 1% O_2 in a hypoxia chamber (SCI-tive Hypoxia Workstation, Baker Ruskinn) or kept in a cell culture incubator at 21% O_2. At depicted time-points, the organoids were recovered from the matrigel and dissolved in 200 µl TE-buffer. After 3 freeze-thaw cycles, the amount of DNA was quantified with Quant-iT™ PicoGreen™ dsDNA Assay Kit (ThermoFisher Scientific) according to the manufacturer's instructions. Absolute values were normalized to the DNA-content 48 hours after seeding.

[^{14}C] 2-Deoxy-D-glucose uptake

For organoid experiments, 3 wells of 50 µl matrigel-embedded organoids per condition were seeded in a 24-well plate. On day 3, cells were kept in normoxia or exposed to hypoxia (at 1% O_2) for 12 hours. The medium was replaced with DMEM containing uniformly-labelled [^{14}C] 2-Deoxy-D-glucose (Hartmann Analytic) at a concentration of 150 µci/mmol and 5 mM glucose. Cells were washed twice with PBS just before harvesting. Radioactivity counts were normalized to cell number.

Illumina RNA sequencing experiment

Multiple organoid lines (5x KPC, 4x KPCS) were seeded as described, where each line was derived from an individual mouse. After 48 hours of exposure to 1% O_2 or 21% O_2, organoids were harvested and RNA was extracted using the NucleoSpin® RNA kit (Macherey-Nagel) according to the manufacturer's instructions. For each organoid line, 2-3 wells of organoids from a 24 well plate were harvested in lysis buffer RA1 (RNA extraction kit, MN) supplemented with TCEP (Tris(2-carboxyethyl)phosphine hydrochloride). For library preparation, the quantity and quality of the isolated RNA was determined with a Qubit® (1.0) Fluorometer (Life Technologies, California, USA) and a Bioanalyzer 2100 (Agilent, Waldbronn, Germany). The TruSeq Stranded mRNA Sample Prep Kit (Illumina, Inc, California, USA) was used in the succeeding steps. Briefly, total RNA samples (1 µg) were ribosome depleted and then reverse-transcribed into double-stranded cDNA with Actinomycin added during first-strand synthesis. The cDNA samples were fragmented, end-repaired and

polyadenylated before ligation of TruSeq adapters. The adapters contain the index for multiplexing. Fragments containing TruSeq adapters on both ends were selectively enriched with PCR. The quality and quantity of the enriched libraries were validated using Qubit® (1.0) Fluorometer and the Bioanalyzer 2100 (Agilent, Waldbronn, Germany). The product is a smear with an average fragment size of approximately 360 bp. The libraries were normalized to 10nM in Tris-Cl 10 mM, pH8.5 with 0.1% Tween 20. Cluster generation and sequencing involved application of the TruSeq SR Cluster Kit v4-cBot-HS or TruSeq PE Cluster Kit v4-cBot-HS (Illumina, Inc, California, USA) using 8 pM of pooled normalized libraries on the cBOT. Sequencing were performed on the Illumina HiSeq 4000 paired end at 2x 100 bp (2x at least 40 million reads) using the TruSeq SBS Kit v4-HS (Illumina, Inc, California, USA).

RNAseq data analysis

The fastq data for the read pairs from the Illumina sequencer has been processed in a bioinformatic workflow. First, the remains of the adapters and sub-standard quality reads have been trimmed with trimmomatic (v0.35). For the pairs in which both reads have passed the trimming, they have been mapped to the mm10 mouse genome using STAR (v2.7.0a) and indexed BAM files obtained with samtools (v1.9). The reads have been counted using featureCounts from subread package (v1.5.0) with the options for pairs of reads to be counted as RNA fragments. The counting used Ensembl v95 mouse genome annotation GTF file. The count vectors for all the samples have been combined into a count table. The table has been processed in the secondary (statistical) analysis with R scripts using edgeR (v3.24.3), in particular binomial generalized log-linear model with contrast tests. It resulted in lists of genes ranked for differential expression by p-value and used Benjamini-Hochberg adjusted p-value as the estimate of the false discovery rate. Read counts are listed in Supplementary Table 1.

Splicing analysis

All splice events were identified using SplAdder on the aligned RNA-Seq BAM files[28]. Gencode release M20 (Mus_musculus.GRCm38.95) was used for identification of slice events. Splice events considered were exon skips, alternative 3'/5', and intron retentions. Only events with highest confidence as defined by SplAdder (level 3) were considered for downstream analyses. All parameters used for the analyses are listed here:

-v y -M merge_graphs -t exon_skip,intron_retention,alt_3prime,alt_5prime -c 3 --ignore_mismatches y

Only events with a minimum of 5 reads and an average expression greater than 20 reads in the flanking exons across all samples were considered in the analysis. All plots and analyses performed on SplAdder output were done in R (version 3.3.3). Intron retention events are listed in Supplementary Table 2.

Statistical analysis

Statistical significance was determined using the statistical tests indicated in the respective figure legends. Data are presented as mean ± SD, if not indicated differently. Mouse studies were not randomized, but were blinded as the analyses were conducted on randomly assigned mouse number, and given to operators without any information until the end of the experiments. Animals of both genders were used and mice with health concerns were excluded from experiments. No inclusion/exclusion criteria were pre-established. No statistical methods were used to predetermine sample size. All experiments are performed at least 3 times if not indicated differently; n refers to the number of biological replicates.

Figure 1

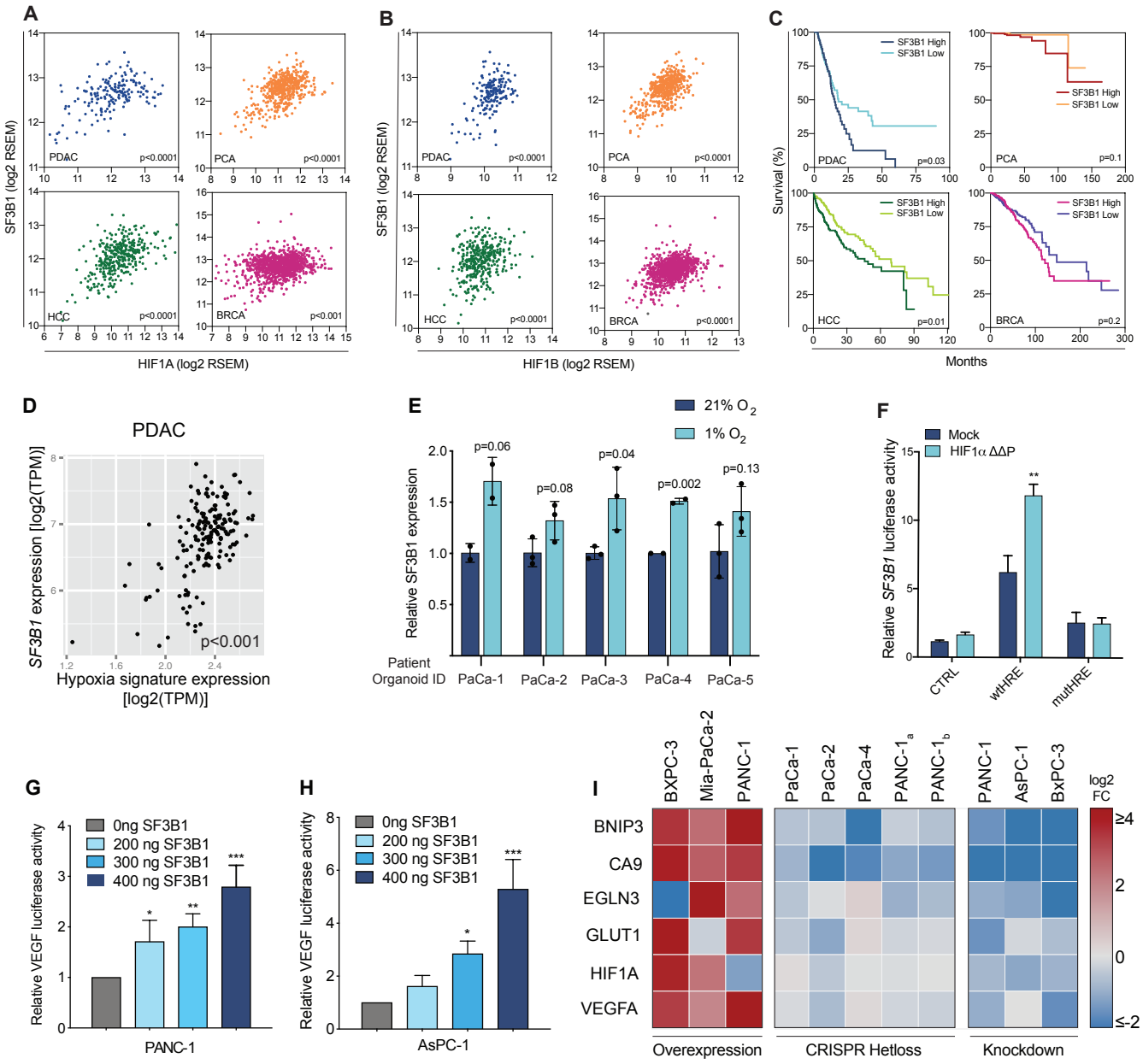

Figure 1. SF3B1 is required for efficient HIF signalling. (A and B) Scatter plot showing the correlation of *SF3B1* and *HIF1A* (A) and *HIF1B* (B) expression in PDAC, prostate cancer (PCA), hepatocellular carcinoma (HCC) and breast cancer (BRCA). The significance of the correlation in is indicated by its p-value. **(C)** Survival of patients was stratified according to the median *SF3B1* expression in the indicated cancer types. P-values were computed with a Log-rank (Mantel-Cox) test. **(D)** Scatter plot showing the correlation between *SF3B1* mRNA levels and a hypoxia signature in PDAC patients, which is represented by the mean expression value (TPM) of 34 HIF-target genes. **(E)** SF3B1 expression in a panel of human patient-derived PDAC organoids exposed to 1% O_2 for 12 hours. Error bars indicate standard deviation (S.D.) of biological replicates. Two-tailed unpaired t-test was used to compute the indicated p-values. **(F)** Transfection of a wildtype (WT) or HRE-mutated *SF3B1* promoter-luciferase reporter together with either an empty vector control, or HIF1αΔΔP in AsPC-1 cells. Data are shown as mean ± S.D. of biological replicates (n=3). ** P<0.01 normalized to mock wtHRE, two-tailed unpaired t-test. **(G and H)** Transfection of a *VEGF* promoter-luciferase reporter alone or together with either HIF1αΔΔP (the constitutively active form of HIF1α), or in combination with different concentrations of SF3B1 plasmid in PANC-1 (G) and AsPC-1 cells (H). Data are shown as mean ± S.D. of biological replicates (n=3). *<P0.05, **P<0.01, ***P<0.001. One-way ANOVA followed by a Dunnet's multiple comparison post-test. **(I)** Heatmap showing the expression of various HIF1α-target genes in patient-derived PDAC organoid lines and commercial PDAC cell lines after overexpression or knockdown of SF3B1, either with CRISPR-Cas9 or siRNA. The indicated fold-changes are relative to the following controls: Transfection with an empty-vector (overexpression), the respective unedited cell line (CRISPR-hetloss) or treatment with control siRNA (knockdown). Expression levels are relative to the housekeeping gene *TBP*. For PANC-1, usage of two distinct guide RNAs are indicated by subscripted *a* and *b*. For each cell line and its respective control, the experiment was performed at least three times.

Figure 2

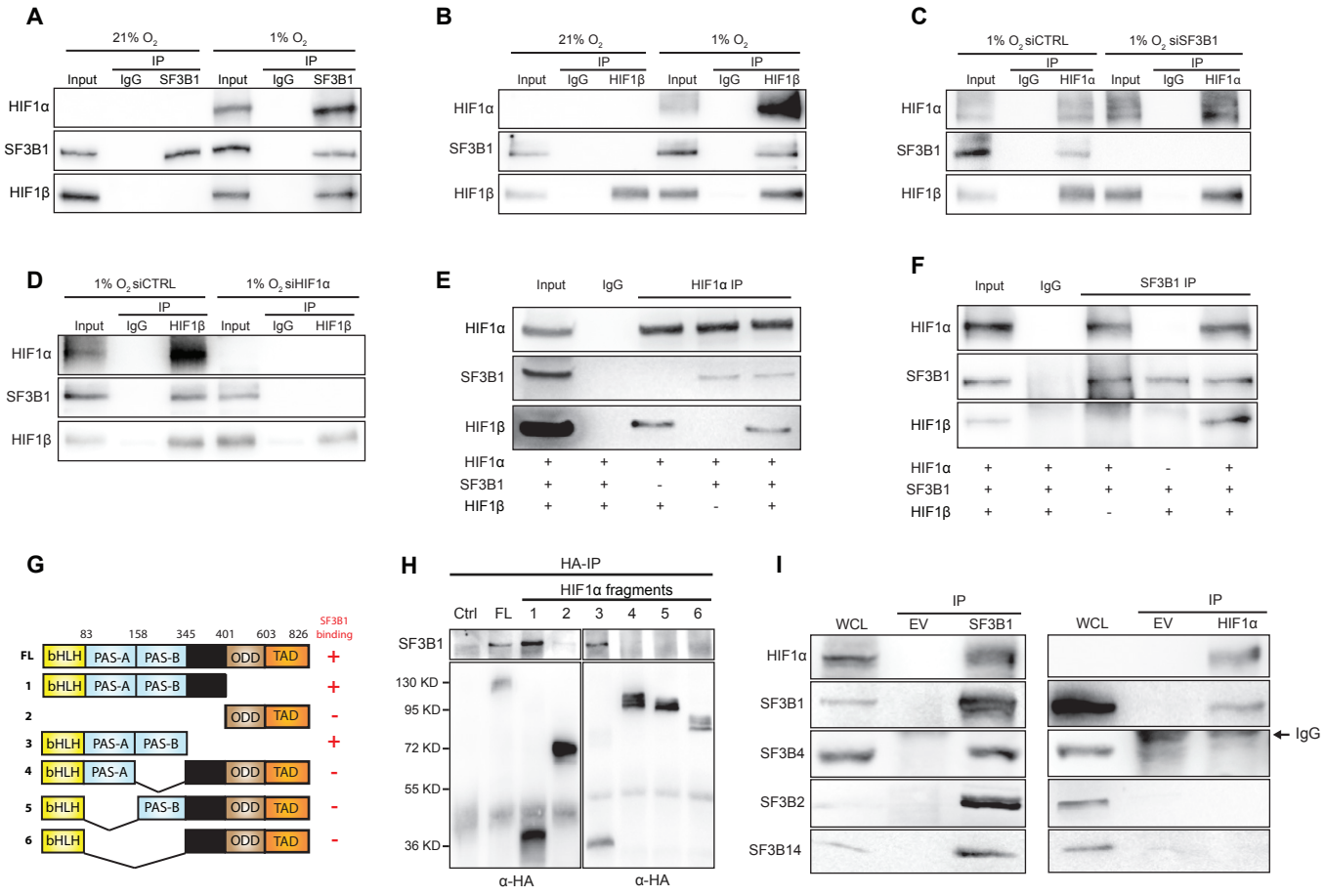

Figure 2. SF3B1 physically interacts with HIF1α. **(A)** Protein extracts from HEK293T cells exposed to 21% or 1% O_2 for 12 hours were subjected to immunoprecipitation (IP) with an anti-SF3B1 antibody or anti-mouse IgG and processed for immunoblotting for indicated proteins. **(B)** Protein extracts from HEK293T cells exposed to 21% or 1% O_2 for 12 hours were subjected to IP with an anti-HIF1β antibody or anti-mouse IgG and processed for immunoblotting for indicated proteins. **(C)** Protein extracts from HEK293T cells transfected with the indicated siRNAs, exposed to 1% O_2 for 12 hours, were subjected to IP with an anti-HIF1α antibody or anti-rabbit IgG and processed for immunoblotting for indicated proteins. **(D)** Protein extracts from HEK293T cells transfected with the indicated siRNAs, exposed to 1% O_2 for 12 hours, were subjected to IP with an anti-HIF1β antibody or anti-rabbit IgG and processed for immunoblotting for indicated proteins. **(E)** Recombinant strep-tagged HIF1α, SF3B1 and HIF1β proteins purified from Sf9 insect cells were mixed and subjected to IP using an anti-HIF1α antibody or anti-rabbit IgG as control and processed for immunoblotting for indicated proteins. (+) means that the indicated recombinant protein was added to the IP, (-) means that the indicated recombinant protein was omitted from the IP. **(F)** Recombinant strep-tagged HIF1α, SF3B1 and HIF1β proteins were subjected to IP using an anti-SF3B1 antibody or anti-mouse IgG as control and processed for immunoblotting for indicated proteins. (+) means that the recombinant protein was added to the IP, (-) means that the recombinant protein was omitted from the IP. **(G)** Schematic of full-length HIF1α and corresponding deletion mutants (numbered 1-6) used in IP experiments with an anti-SF3B1 antibody. (+) and (-) signs denote SF3B1 binding (experimental data are displayed in Fig. 2H). bHLH: basic helix-loop-helix, PAS-A and PAS-B: Per-ARNT-Sim domains, ODD: oxygen-dependent degradation domain and TAD: transactivation domain. **(H)** HEK293T cells were transfected with a HA-tagged WT full length (FL) or mutant forms of HIF1α (1-6). Lysates were then processed for immunoprecipitation with an anti-HA antibody (HA-IP) followed by immunoblotting with an anti-HA antibody. **(I)** Protein extracts from HEK293T cells exposed to 1% O_2 for 8 hours were subjected to IP, with an anti-SF3B1 antibody or an anti-mouse IgG (left), or with an anti-HIF1α antibody and an anti-rabbit IgG (right). All samples were processed for immunoblotting for indicated proteins. The arrow on the right indicates the IgG band.

Figure 3

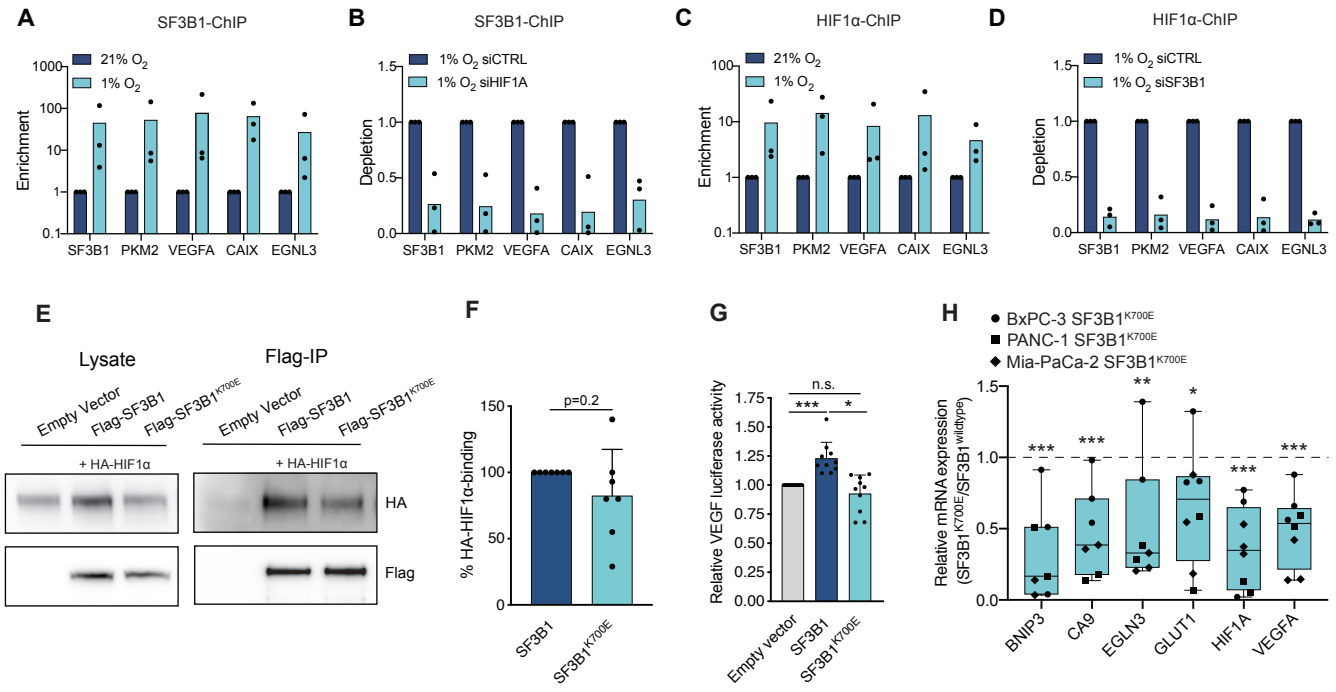

Figure 3. SF3B1 increases binding of HIF1α to its target genes. (A and B) Chromatin immunoprecipitation (ChIP) using a specific antibody against SF3B1 in HEK293T cells. (A) Cells are cultured under 21% or 1% O_2 for 8 hours. The fold-increase in target gene binding under hypoxia is shown relative to normoxia. (B) Cells are transfected with siRNA targeting HIF1α or scrambled siRNA, and incubated in 1% O_2 for 8 hours. The decrease in target gene binding in HIF1α-siRNA treated cells is shown relative to the control. **(C and D)** Chromatin immunoprecipitation (ChIP) using a specific antibody against HIF1α in HEK293T cells. (C) Cells are cultured under 21% or 1% O_2 for 8 hours, the fold-increase in hypoxia is shown relative to normoxia. (D) Cells are transfected with siRNA targeting SF3B1 or scrambled siRNA, and incubated in 1% O_2 for 8 hours. The decrease in target gene binding in SF3B1-siRNA treated cells is shown relative to the control. (A – D) Results show three independent experiments. **(E)** Representative Western-blot of the Co-IP of HA-tagged HIF1α and FLAG-tagged wildtype SF3B1, and its variant K700E. **(F)** Quantification of HA-tagged HIF1α in HEK293T cells, pulled down with the indicated SF3B1 variants. The data are represented as mean ± S.D. of independent experiments (n = 7). P-value was calculated by a two-tailed unpaired t-test. **(G)** Transfection of the indicated constructs in HEK293T cells stably expressing a HIF-luciferase reporter. Data are shown as mean ± S.D. of biological replicates, indicated by data points. *<P0.05, **P<0.01, ***P<0.001, two-tailed unpaired t-test. Data are normalized to transfection of an empty vector construct. **(H)** qPCR analysis of HIF-target genes in the indicated cell lines overexpressing *SF3B1*^{K700E} after exposure to 1% O_2 for 8 hours. Data are normalized to the respective cell lines overexpressing wildtype *SF3B1* after exposure to 1% O_2 for 8 hours. Expression levels are relative to the housekeeping gene *TBP* (n = 2-3). Each data point represents an individual experiment of the depicted cell line. * P<0.05, ** P<0.01, *** P<0.001, two-tailed unpaired t-test.

Figure 4

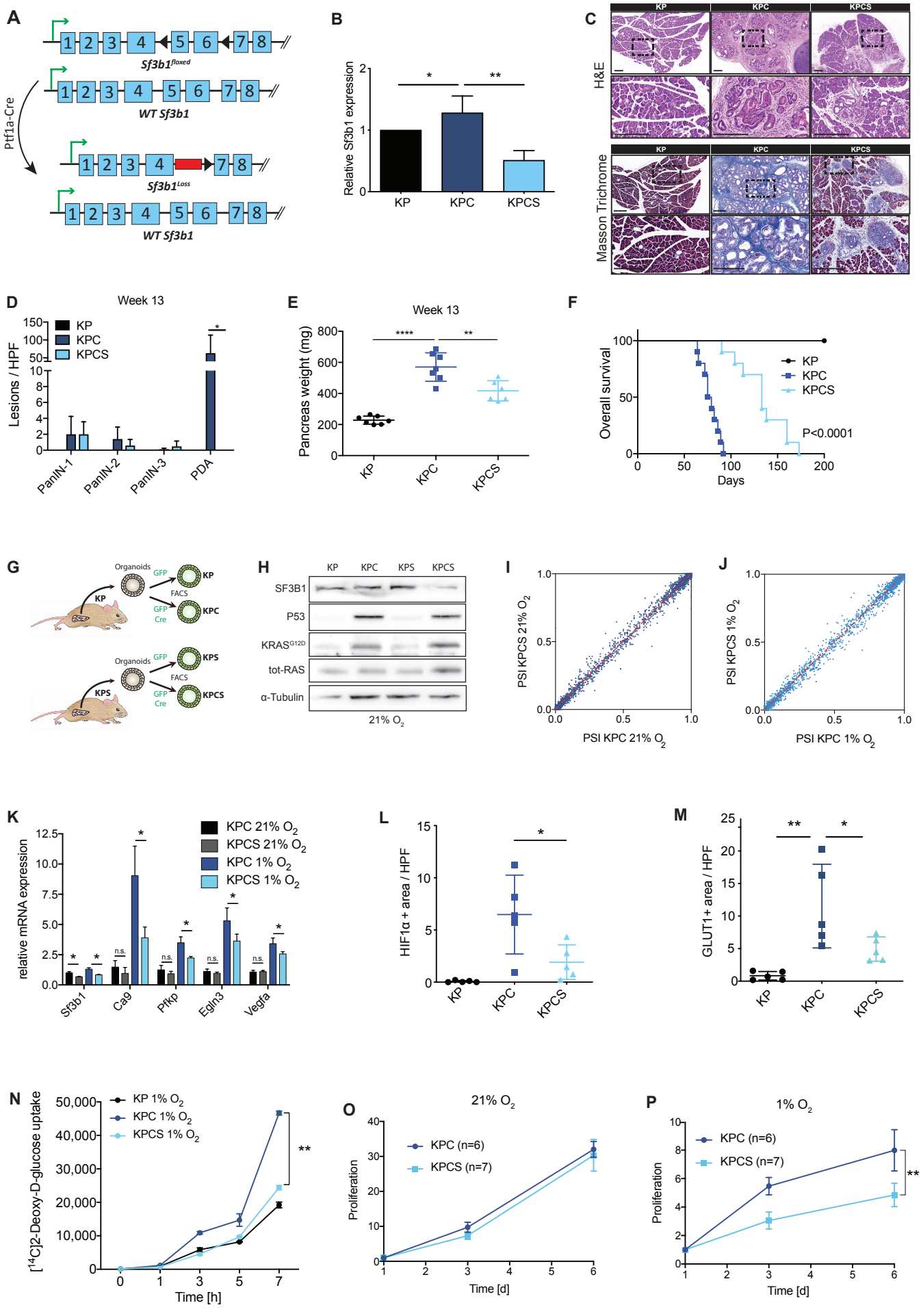

Figure 4. Heterozygosity of *Sf3b1* hampers PDAC progression through impaired HIF-signalling. (A) Schematic representation of the transgenic approach to obtain pancreas-specific heterozygosity of Sf3b1. **(B)** qPCR analysis of *Sf3b1* mRNAs from pancreata of KP, KPC and KPCS mice of 13 weeks of age. For *P<0.05 **P<0.01. One-way ANOVA followed by a Tukey's multiple comparison post-test. **(C)** Representative images of H&E staining and Masson's Trichrome staining showing histopathologic lesions in pancreata of KP, KPC and KPCS mice at 13 weeks of age. Dashed lines indicate the area magnified below. Scale bar is 100 μm. **(D)** Quantification of the prevalence of mPanIN and PDAC in the H&E-stained pancreatic sections of 13-week-old KP, KPC and KPCS mice. Ten high power fields (HPF) were analysed per animal. Data are represented as mean ± S.D. (n = 5). * P<0.05, ** P<0.01, *** P<0.001. One-way ANOVA followed by a Tukey's multiple comparison post-test. **(E)** Pancreas weight of 13 weeks old KP, KPC and KPCS mice. The data are represented as mean ± S.D. (n = 6-7). ** P<0.01, **** P<0.0001. One-way ANOVA followed by a Tukey's multiple comparison post-test. **(F)** Kaplan-Meier survival curve of KP, KPC and KPCS mice over time (KP n = 8, KPC n = 10, KPCS n = 10). Long rank test. **(G)** Schematic representation of the generation of murine tumor organoids with GFP or GFP-Cre viruses derived from KP and KPS mice. Expression of Cre recombinase in KPC and KPCS organoids leads to the activation of $Kras^{G12D}$ and $Trp53^{R17H}$ and to a loss of one allele of *Sf3b1* in KPCS organoids. **(H)** Protein extracts from KP, KPC, KPS, and KPCS organoids grown under normoxic conditions were immunoblotted for the indicated proteins. **(I and J)** Scatter plot of percent spliced-in (PSI) events in KPC and KPCS organoids cultured in normoxia (G) and hypoxia (H), representing a measure of high confidence alternative splice events (n ≥ 4 organoid lines, lines established from individual mice). **(K)** Expression levels of HIF1α target genes determined by qPCR of KPC and KPCS organoids (n = 6 organoid lines) cultured in normoxia and hypoxia for 48 hours. Expression levels are relative to the housekeeping gene *Actb*. Data are shown as mean ± SEM. For each organoid line, the experiment was performed in three biological replicates. * P<0.05, One-way ANOVA followed by a Tukey's multiple comparison post-test. **(L and M),** Quantification of HIF1α (L) or GLUT1 (M) positive areas in KP, KPC and KPCS mice at 13 weeks of age. Ten high power fields (HPF) were analysed per animal (n = 5). * P<0.05. One-way ANOVA followed by a Tukey's multiple comparison post-test. (**N**) KPC and KPCS organoids were incubated in medium containing [^{14}C] 2-deoxyglucose at different time-points and processed for glucose uptake measurements. Organoids were exposed to 1% O_2 for 12 hours. Counts were normalized to the cell number (n = 4 biological replicates per time point and condition). ** P<0.01, One-way ANOVA followed by a Tukey's multiple comparison post-test. **(O and P)** Proliferation of organoids in normoxia (O) and hypoxia (P). Data are shown as mean ± SEM of organoid lines (n ≥ 6 organoid lines). For each organoid line, the experiment was performed in three biological replicates. ** P<0.01, indicating comparison of KPC and KPCS, Two-way ANOVA followed by a Sidak's multiple comparisons test.

Figure 5

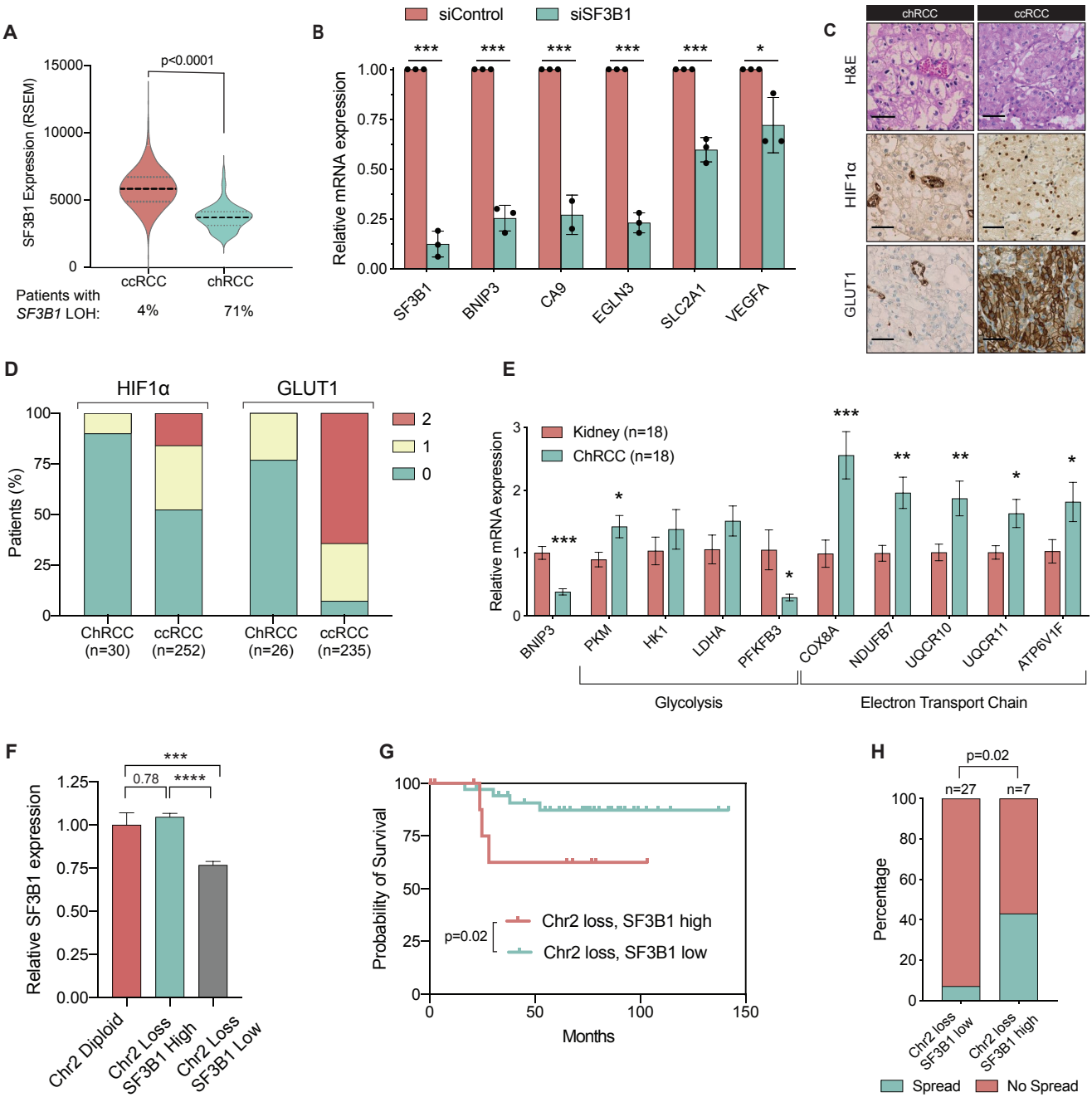

Figure 5. ChRCC with heterozygous SF3B1 loss grows in a normoxic environment. (A) Expression of SF3B1 and loss of heterozygosity (LOH) in clear cell renal cell carcinoma (ccRCC) and chromophobe renal cell carcinoma (chRCC) based on TCGA data. One-way ANOVA followed by a Tukey's multiple comparison post-test. **(B)** qPCR analysis of indicated genes in patient-derived cell chRCC cells treated with siControl or siSF3B1 under 1% O_2 for 8 hours. Data represents results of three independent experiments. Expression levels are relative to the housekeeping gene *TBP*. * P<0.05, *** P<0.001, two-tailed unpaired t-test. **(C)** Representative H&E and IHC staining of HIF1α and GLUT1 of ccRCC and chRCC patients, scale bar is 50μm. **(D)** Quantification of HIF1α and GLUT1 staining in ccRCC and chRCC patients, categorized as intense (2), weak (1) or no detectable (0) staining. **(E)** qPCR analysis of genes involved in glycolysis and oxidative phosphorylation in chRCC tumors (n = 18) and matched kidney tissue (n = 18). Expression levels are relative to *TBP*. * P<0.05, ** P<0.01, *** P<0.001, two-tailed unpaired t-test. **(F)** Relative SF3B1 expression of the stratified TCGA-cohort. *** P<0.001, **** P<0.0001. One-way ANOVA followed by a Tukey's multiple comparison post-test. **(G)** Survival of patients (TCGA cohort) stratified according to chromosome 2 status and SF3B1 expression as indicated. P-value was computed with a Log-rank (Mantel-Cox) test. **(H)** Percentage of chRCC patients (TCGA cohort) where spreading to lymph nodes was observed. Patients lacking information of lymph node status were omitted for analysis. Significance was computed with chi-square tests.

Supplementary Figure 1

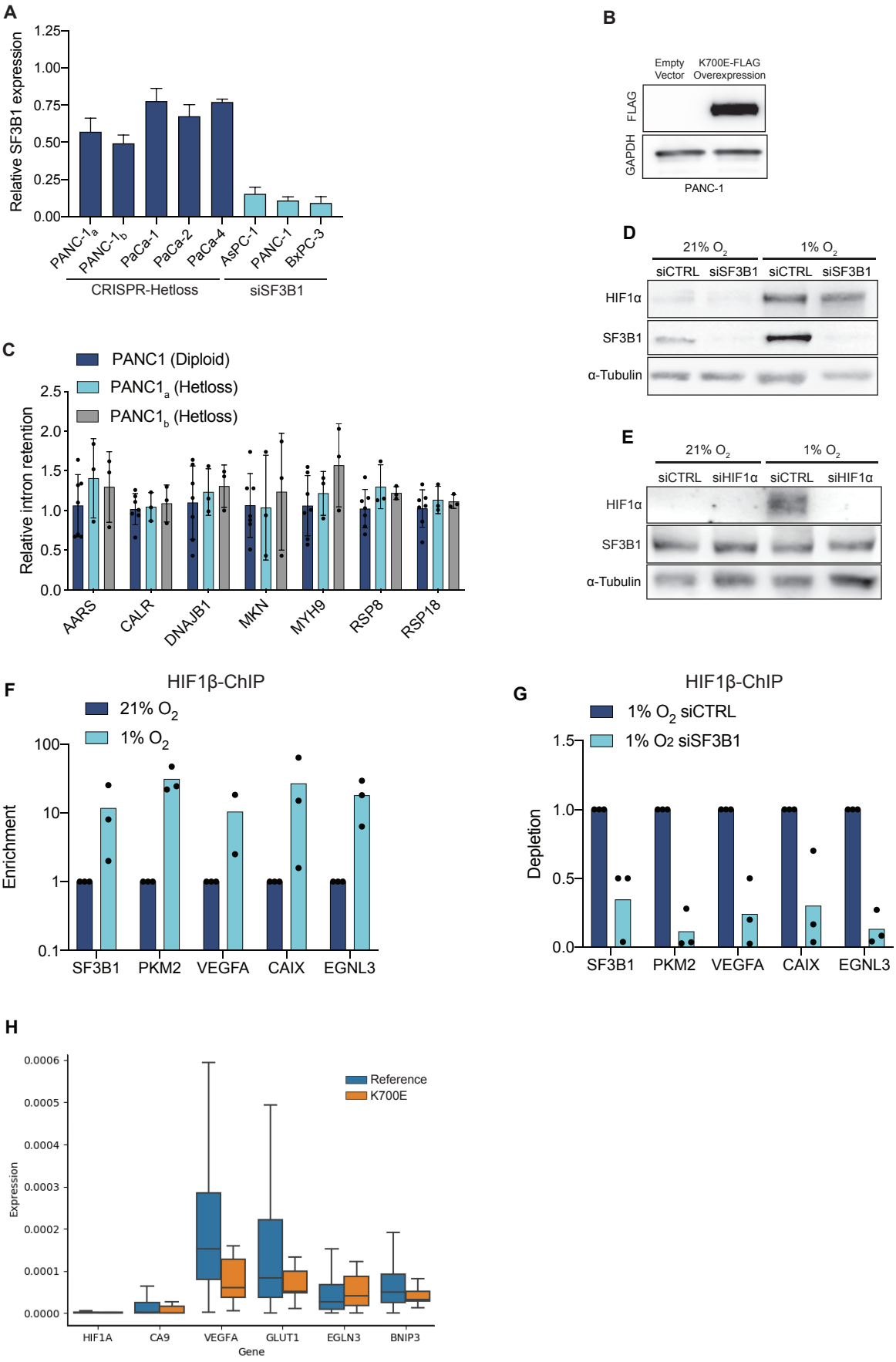

Supplementary Figure 1. Effects of SF3B1 reduction on HIF-response. (A) Relative SF3B1expression in the indicated patient-derived organoids and cell lines, engineered with CRISPR-Cas9 (mono-allelic loss of *SF3B1*) or treated with siRNA, and measured by qPCR. In PANC-1 cells, two different guide RNAs were used to target *SF3B1*. Data are shown as mean ± S.D. of biological replicates (n = 3). The data is normalized to the respective unedited cell line (CRISPR-Hetloss) or treatment with control siRNA. Expression levels are relative to *TBP*. **(B)** Western blot analysis for FLAG in protein extracts from PANC-1 cells overexpressing FLAG-tagged SF3B1. **(C)** Intron retention assessed by qPCR; expression levels are relative to the housekeeping gene *TBP*. Data are shown as mean ± S.D. of biological replicates (n ≥ 3). **(D and E)** Protein extracts from HEK293T cells treated with siRNA targeting SF3B1 (D) or HIF1α (E), exposed to 21% or 1% O_2 for 12 hours and processed for immunoblotting for the indicated proteins. **(F)** Chromatin immunoprecipitation (ChIP) from HEK293T cells cultured under 21% or 1% O_2 for 8 hours using a specific antibody against HIF1β. The fold-increase in hypoxia is shown relative to normoxia. (**G**) Cells were transfected with siRNA targeting SF3B1 or scrambled siRNA, and incubated in 1% O_2 for 8 hours. The decrease in target gene binding in SF3B1-siRNA treated cells is shown relative to the control. (F, G) Results show three independent experiments. **(H)** Pan-cancer analysis of selected HIF-target genes in patient samples with $SF3B1^{K700E}$ or *SF3B1-WT* (reference). Only solid cancers in the TCGA database were used for analysis (reference = 8243 samples; $SF3B1^{K700E}$ = 12 samples).

Supplementary Figure 2

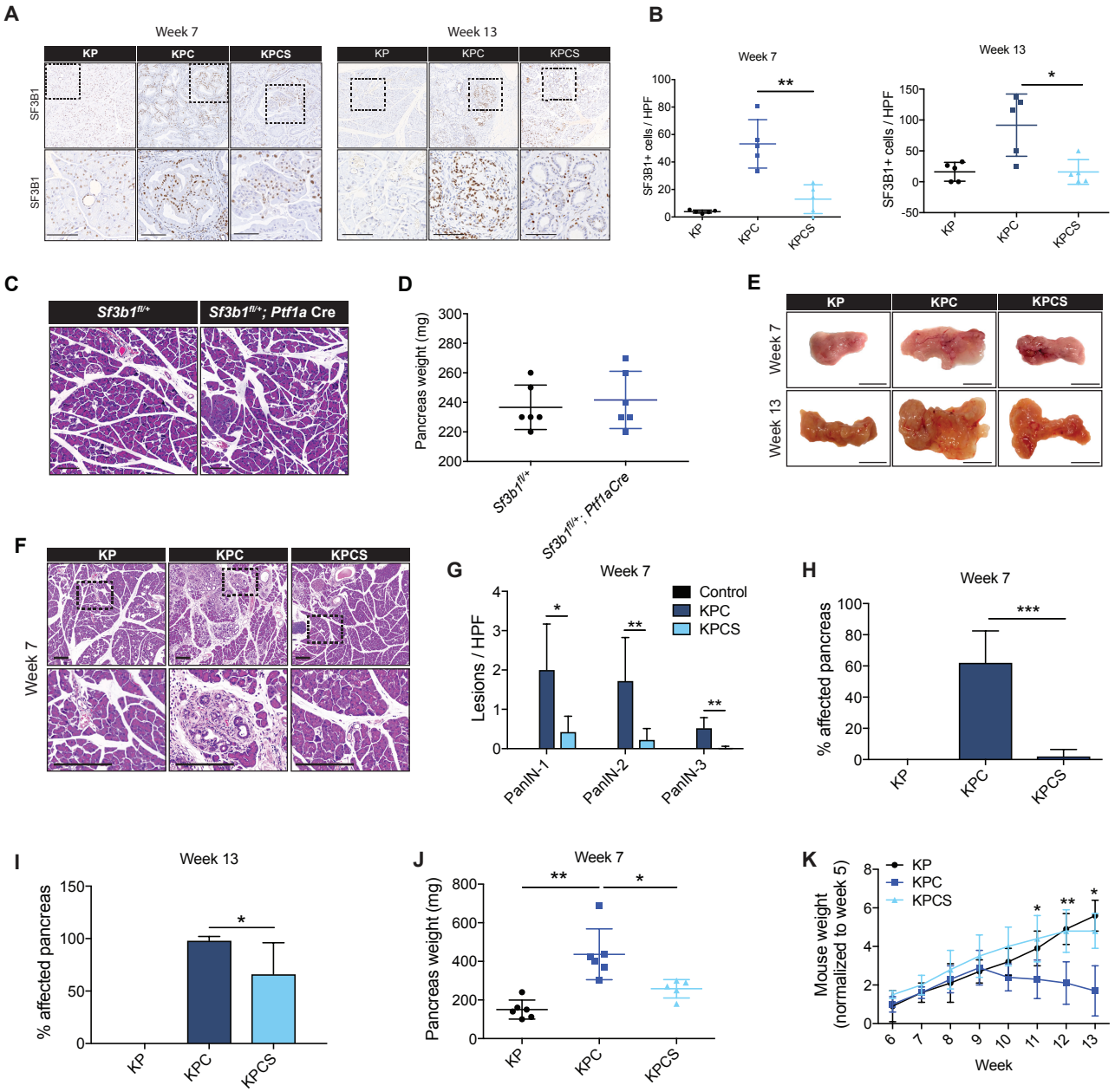

Supplementary Figure 2. Effect of SF3B1 reduction on PDAC growth. (A) Representative immunohistochemical staining for SF3B1 in pancreata from 7- and 13-week old KP, KPC and KPCS mice. Dashed lines indicate the area magnified below. Scale bar is 100 µm. **(B)** Quantification of SF3B1 positive areas in KP, KPC and KPCS mice at 7 and 13 weeks of age. Ten high power fields (HPF) were analysed per animal (n = 5). * P<0.05. One-way ANOVA followed by a Tukey's multiple comparison post-test. **(C)** H&E staining of pancreata from *Sf3b1*$^{fl/+}$ and *Sf3b1*$^{fl/+}$*; Ptf1aCre* mice at 13 weeks of age. Representative images, scale bar is 100 µM. **(D)** Evaluation of pancreas weight of *Sf3b1*$^{fl/+}$ and *Sf3b1*$^{fl/+}$*; Ptf1aCre*, mice at 13 weeks of age. The data are represented as mean ± S.D. (n = 6-7). **(E)** Representative photographs of KP, KPC, and KPCS pancreata from 13 weeks-old mice. Scale bar: 1cm. **(F)** Representative images of H&E staining revealing the histopathologic lesions in pancreata of KP, KPC and KPCS mice at the indicated age. Square dashed lines indicate the area magnified in the image below. Scale bar is 100 µm. **(G – I)** Quantification of the prevalence of mPanIN and PDAC in the H&E-stained pancreatic sections of 7-week-old KP, KPC and KPCS mice (G). Quantification of the affected pancreas at the indicated age (H, I). Ten high power fields (HPF) were analysed per animal. The data are represented as mean ± S.D. (n = 5). * P<0.05, ** P<0.01, *** P<0.001. One-way ANOVA followed by a Tukey's multiple comparison post-test. **(J)** Pancreas weight of KP, KPC and KPCS mice at 7 weeks of age. The data are represented as mean ± S.D. (n = 6-7). * P<0.05, ** P<0.01, *** P<0.001. One-way ANOVA followed by a Tukey's multiple comparison post-test. **(K)** Body weight of KP, KPC, and KPCS mice at indicated time point over a period of 13 weeks. The data are normalized to body weight of the mice at 5 weeks of age and represented as mean ± S.D. (n = 6-8). * P<0.05, ** P<0.01. One-way ANOVA followed by a Tukey's multiple comparison post-test.

Supplementary Figure 3

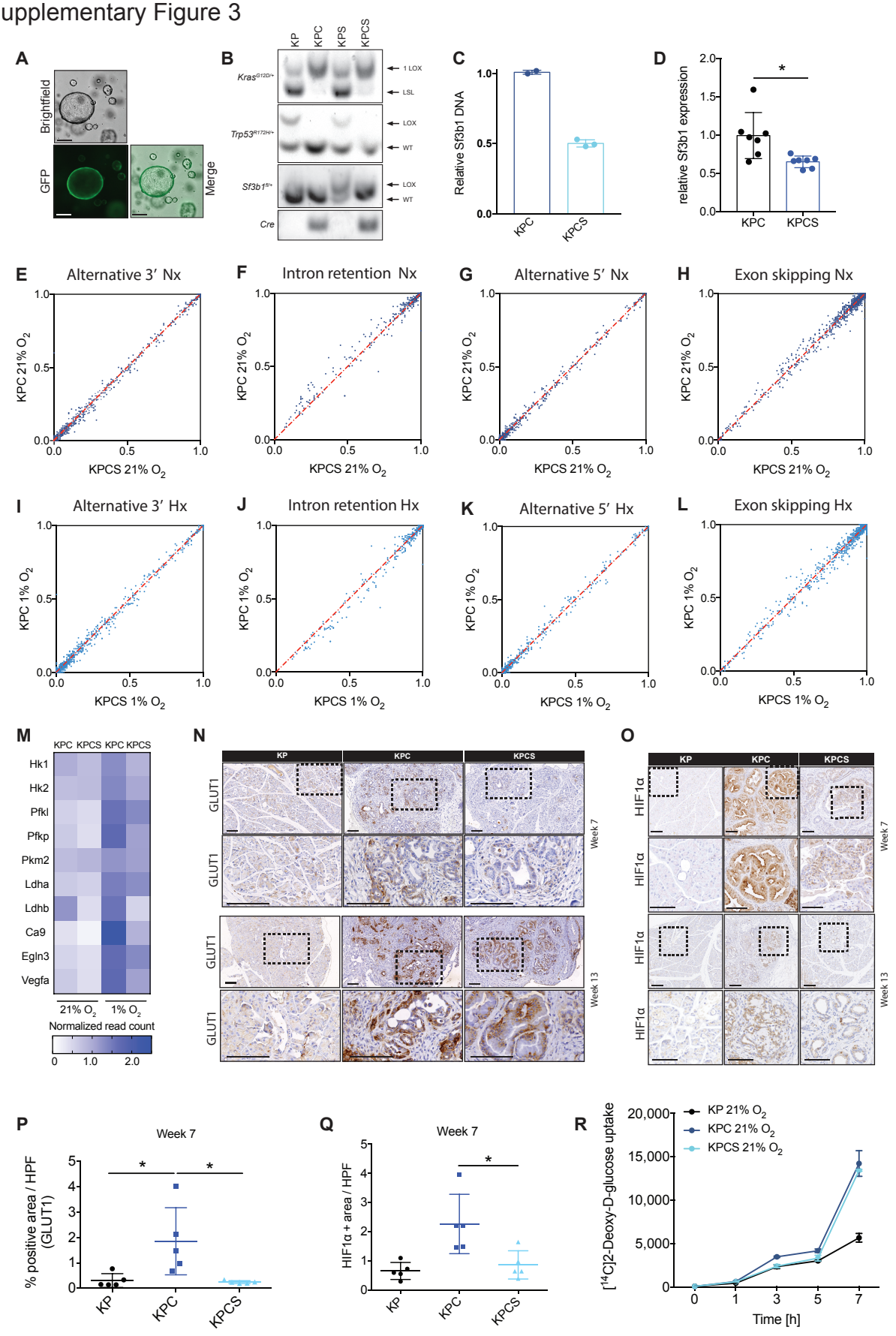

Supplementary Figure 3. *Sf3b1* heterozygosity affects PDAC growth via HIF signalling. (A) Bright field and fluorescence images of mouse organoids transduced with a GFP-Cre virus after FACS. **(B)** Representative PCR analysis of genomic DNA from KP, KPC, KPS and KPCS organoids. The Cre-mediated recombination of the conditional allele *KrasG12D/+*, *Trp53R172H/+* generates a single LoxP site and 2 LoxP sites for *Sf3b1*. (**C**) *Sf3b1* DNA levels at exon 5 for validation of monoallelic Sf3b1 knockout in the indicated organoid lines assessed by qPCR. Values were normalized to *Sf3b1* exon 2 DNA levels, which remain unaffected by Cre-lox recombination. **(D)** *Sf3b1* mRNA expression of KPC and KPCS organoid lines. *P<0.05, ** P<0.01, two-tailed unpaired t-test. **(E-L)** Scatter plot of alternative 3' end usage (E, I), intron retention (F, J), alternative 5' end usage (G, K) and exon skipping (H, L) events in KPC and KPCS organoids cultured in normoxia (E to H) and hypoxia (I to L). Events were computed by SplAdder[29], only high confidence events were considered for the analyses. **(M)** Heatmap displaying normalized read counts for the indicated genes derived by RNA-sequencing. **(N)** Representative immunohistochemical staining for GLUT1 in pancreata from 7-week and 13-week old KP, KPC and KPCS mice. Dashed lines indicate the area magnified below. Scale bar: 100 µm. **(O)** Representative immunohistochemical staining for HIF1α in pancreata from 7-week and 13-week old KP, KPC and KPCS mice. Dashed lines indicate the area magnified below. Scale bar: 100 µm. **(P)** Quantification of GLUT1 positive areas in KP, KPC and KPCS mice at 7 weeks of age. Ten high power fields (HPF) were analysed per animal (n = 5). * P<0.05. One-way ANOVA followed by a Tukey's multiple comparison post-test. **(Q)** Quantification of HIF1α positive areas in KP, KPC and KPCS mice at 7 weeks of age. Ten high power fields (HPF) were analysed per animal (n = 5). * P<0.05. One-way ANOVA followed by a Tukey's multiple comparison post-test. **(R)** KPC and KPCS organoids were incubated in normoxic conditions in medium containing [^{14}C]-2-deoxyglucose at different time-points and processed for glucose uptake measurements. Counts were normalized to the cell number (n = 4 biological replicates per time point and condition). ** P<0.01, One-way ANOVA followed by a Tukey's multiple comparison post-test.

Supplementary Figure 4

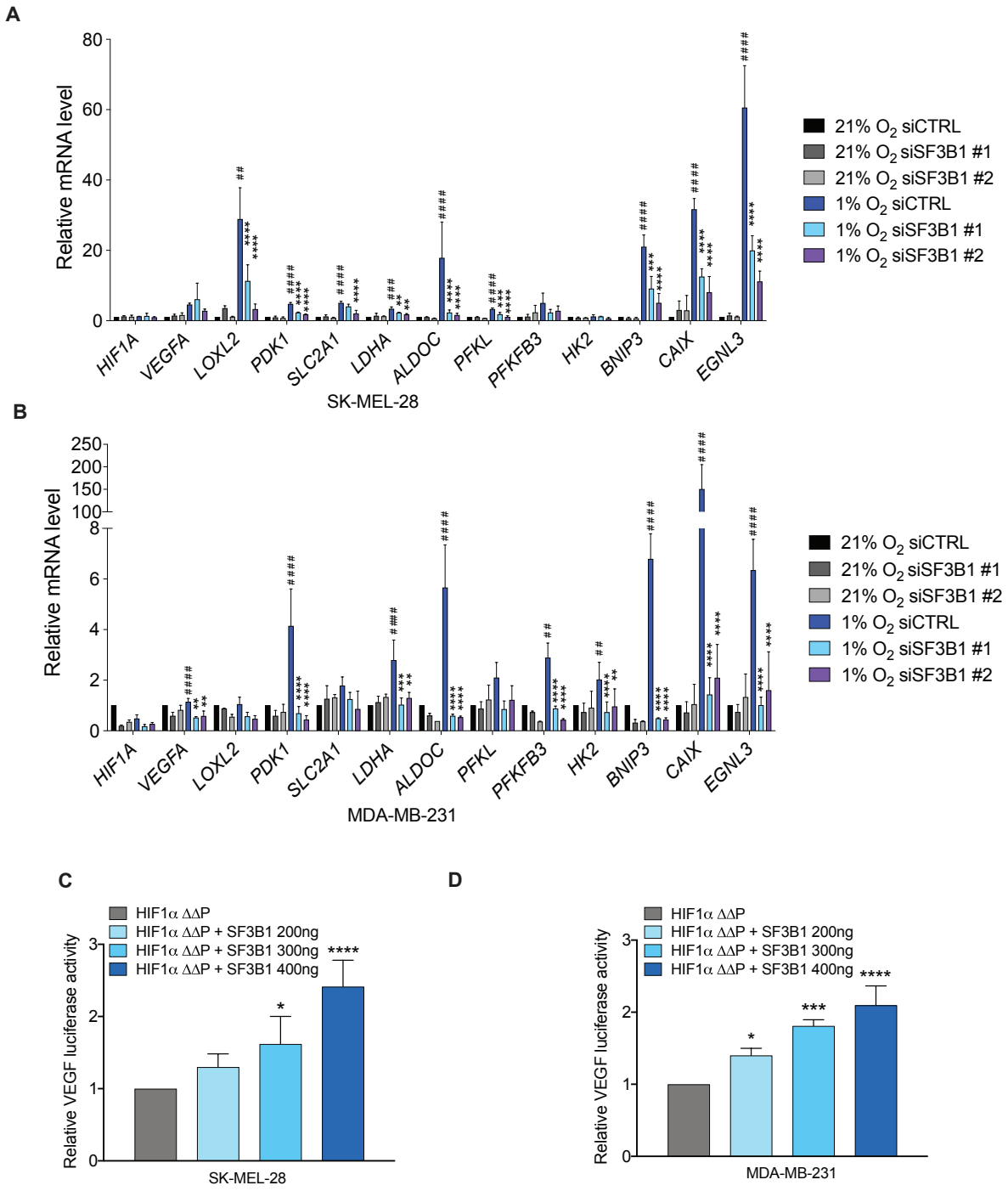

Supplementary Figure 4. SF3B1 reduction affects HIF signalling in various cancer cell lines. (A and B) qPCR analyses of the indicated genes in SK-MEL-28 (A) and MDA-MB-231 (B), transfected with the depicted siRNAs and incubated in 21% or 1% O_2 for 12 hours. Expression levels are relative to *TBP*. Data are shown as mean ± S.D. of biological replicates (n=3). *P<0.05, **P<0.01, ****P<0.0001, data normalized to 1% O_2 siCTRL. For # P<0.05, ## P<0.01, #### P<0.0001, data are normalized to 21% O_2 siCTRL. Two-tailed unpaired t-test. **(C and D)** Transfection of a *VEGF* promoter-luciferase reporter alone or together with either HIF1αΔΔP (the constitutively active form of HIF1α), or in combination with different concentrations of SF3B1 plasmid in SK-MEL-28 (C) and MDA-MB-231 cells (D). Data are shown as mean ± S.D. of biological replicates (n = 3). *<P0.05, **P<0.01, ***P<0.001, **** P<0.0001. One-way ANOVA followed by a Dunnet's multiple comparison post-test.

Supplementary Figure 5

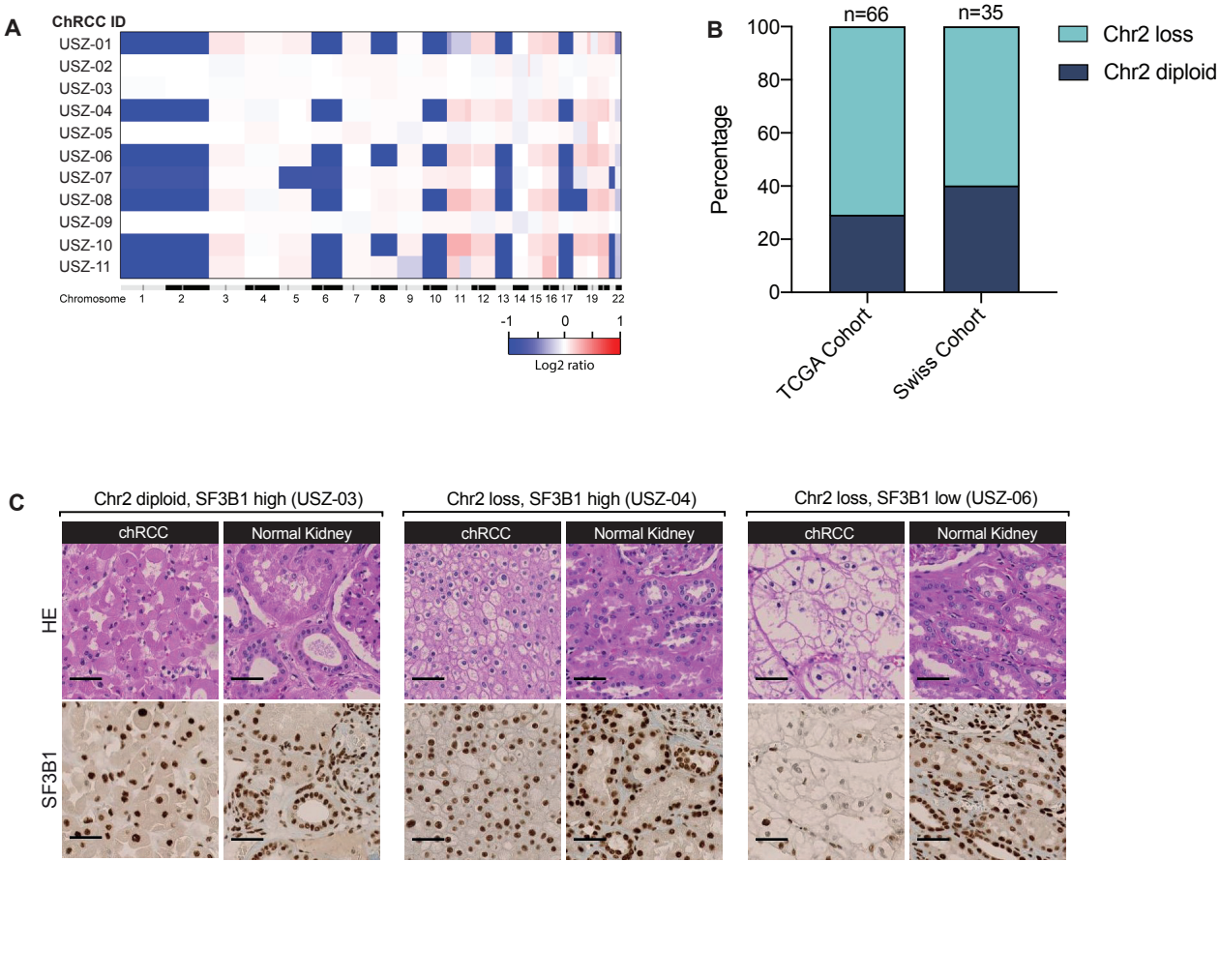

Supplementary Figure 5. *SF3B1* heterozygosity is frequently observed in chRCC. (A) Copy number variations (CNV) analysed with array-based comparative genome hybridization (array-CGH) of tumors from 11 chRCC patients of the Swiss-cohort. **(B)** Chromosome 2 status in chRCC samples of the TCGA cohort and the Swiss cohort. The Swiss cohort is composed of samples published by Ohashi et al.[24] (n=24) and the samples shown in Suppl. Fig. 5A (n=11). **(C)** Representative H&E and IHC staining of SF3B1 chRCC patients without loss (left) and with loss (middle and right) of chromosome 2. The middle staining shows compensation of heterozygous loss of *SF3B1*, whereas the sample on the right has reduced levels of SF3B1. Scale bar is 50µm.